Cell

Immunometabolic defects of CD8+ T cells disrupt gut barrier integrity in people with HIV

Graphical abstract

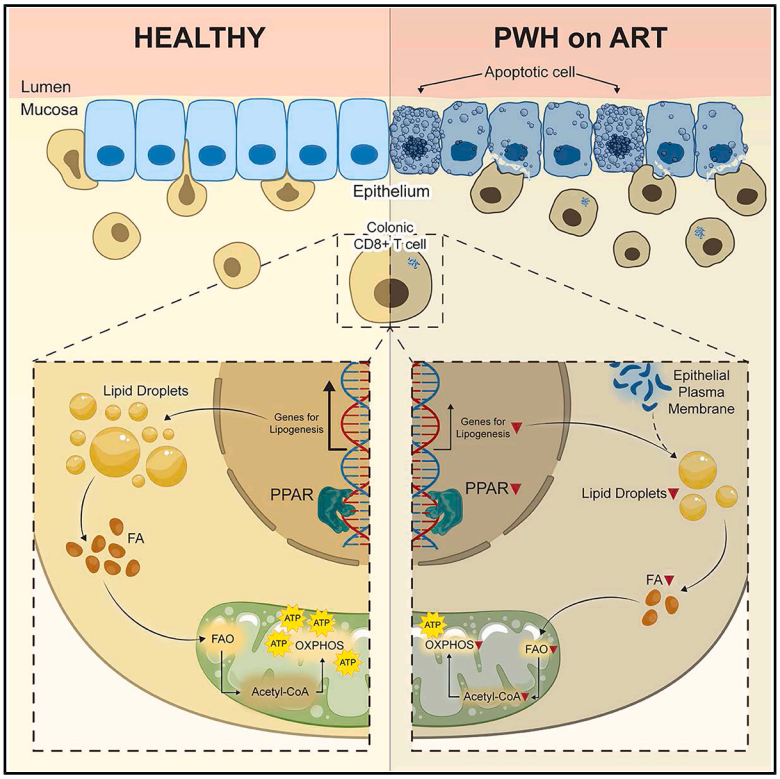

Highlights

- Lipid metabolism of colon CD8$^+$ T cells is disrupted by PPARγ loss in PWH on ART
- PPARγ-deficient colon CD8$^+$ T cells induce epithelial apoptosis
- Treatment with a PPARγ agonist restores lipid homeostasis in colon CD8$^+$ T cells
- CD8$^+$ T cell PPAR signaling is essential for intestinal barrier function

Authors

Upasana Das Adhikari, Leah M. Froehle, Alexandra N. Pipkin, ..., Alison E. Ringel, Ömer H. Yilmaz, Douglas S. Kwon

Correspondence

udasadhikari@mgh.harvard.edu (U.D.A.), dkwon@mgh.harvard.edu (D.S.K.)

In brief

PPARγ downregulation in colonic CD8+ T cells from people with HIV (PWH) on antiretroviral therapy (ART) disrupts lipid metabolism and promotes contact-dependent epithelial apoptosis, leading to intestinal barrier dysfunction. Pharmacological activation of PPARγ restores metabolic fitness and reduces epithelial damage, revealing a potential therapeutic target for mucosal repair in PWH.

Das Adhikari et al., 2025, Cell *188*, 5666–5679
October 2, 2025
https://doi.org/10.1016/j.cell.2025.08.024

CellPress

CellPress
OPEN ACCESS

Cell

Article

Immunometabolic defects of CD8+ T cells disrupt gut barrier integrity in people with HIV

Upasana Das Adhikari,[1,*] Leah M. Froehle,[1] Alexandra N. Pipkin,[1] Heeva Baharlou,[1] Alice H. Linder,[1] Palak Shah,[1] Amanda Hussey,[2] Qiming Zhang,[2] Sarah Nyquist,[1] Saleh Khawaled,[2] Fangtao Chi,[2] Swagata Goswami,[2] Sabhyata Sedhain,[2] Salina Hussain,[1] Thomas J. Diefenbach,[1] Benjamin J. Read,[1] Byungji Kim,[2] Darrell Irvine,[2] Osaretin Asowata,[3] Mark Ladinsky,[4] Pamela Bjorkman,[4] Fusi Madela,[3] Shakeel Kader,[3] Alex K. Shalek,[1] Musie Ghebremichael,[1] Henrik Kloverpris,[3] Alison E. Ringel,[1,2] Ömer H. Yilmaz,[2] and Douglas S. Kwon[1,5,6,*]

[1]Ragon Institute of Mass General Brigham, MIT and Harvard, Cambridge, MA 02139, USA
[2]Koch Institute, Massachusetts Institute of Technology, Cambridge, MA 02139, USA
[3]Africa Health Research Institute, University of KwaZulu Natal, Durban 4001, South Africa
[4]California Institute of Technology, Pasadena, CA 91125, USA
[5]Division of Infectious Diseases, Massachusetts General Hospital, Boston, MA 02114, USA
[6]Lead contact
*Correspondence: udasadhikari@mgh.harvard.edu (U.D.A.), dkwon@mgh.harvard.edu (D.S.K.)
https://doi.org/10.1016/j.cell.2025.08.024

SUMMARY

A hallmark of HIV infection is disruption of intestinal barrier integrity that persists in people with HIV (PWH) despite treatment with antiretroviral therapy (ART). This disruption is central to HIV disease progression, yet the causes remain incompletely understood. We report a mechanism by which immunometabolic defects in colon-resident CD8$^+$ T cells in PWH lead to intestinal epithelial apoptosis and disruption of intestinal barrier integrity. We show that in PWH, these cells downregulate the lipid sensor peroxisome proliferator-activated receptor-γ (PPARγ), which results in reduced intracellular lipid droplets, impaired fatty acid oxidation, and acquisition of lipids by CD8$^+$ T cells from intestinal epithelial cells, which then contributes to epithelial cell death. Our findings indicate that HIV-associated immunometabolic dysregulation of colon CD8$^+$ T cells leads to loss of intestinal epithelial homeostasis. These results identify potential strategies to reduce comorbidities in PWH and other disorders with disrupted intestinal barrier integrity.

INTRODUCTION

Intestinal barrier breakdown is a hallmark of HIV infection, which persists even after long-term treatment with suppressive antiretroviral therapy (ART).[1,2] This intestinal barrier disruption results in translocation of luminal microbial products into the circulation, triggering chronic systemic immune activation[1,3–7] and significantly contributing to the development of HIV-associated noncommunicable diseases (NCDs), such as diabetes, obesity, cardiovascular disease, and stroke.[8,9] Although ART has significantly improved the lives of people with HIV (PWH), the heightened burden of NCDs continues to increase morbidity and mortality in this population.[10,11] Similar observations of loss of intestinal barrier integrity and chronic inflammation have been made in individuals with inflammatory bowel disease (IBD) and other intestinal inflammatory conditions.[5,6,12,13] Despite this, the mechanisms governing intestinal barrier disruption remain poorly understood. The maintenance of intestinal barrier integrity relies on the regeneration of intestinal epithelial cells, which undergo continuous proliferation and differentiation. This process is influenced by external signals from both epithelial and non-epithelial cells, particularly stromal cells and tissue-resident immune cells.[13–17] Studies suggest T cells play an important role in maintaining tissue homeostasis, including surveying the epithelium and eliminating intestinal epithelial stem cells with aberrant behavior through interactions with MHC class I.[18,19] However, the potential role of resident T cells in the maintenance or disruption of the intestinal epithelium in PWH is incompletely understood.

In this study, we identify a mechanism by which colon tissue-resident memory (TRM) CD8$^+$ T cells contribute to impaired intestinal barrier integrity in PWH on ART. Using endoscopic biopsies from human subjects, we show increased colon epithelial cell apoptosis *in vivo* and in patient-derived organoids from PWH. Our results indicate that colon TRM CD8$^+$ T cells in PWH on ART downregulate expression of the lipid sensor peroxisome proliferator-activated receptor-γ (PPARγ), which leads to impaired cellular lipid metabolism. This metabolic dysregulation of colon-resident CD8$^+$ T cells contributes to intestinal epithelial cell apoptosis through a non-canonical interaction between

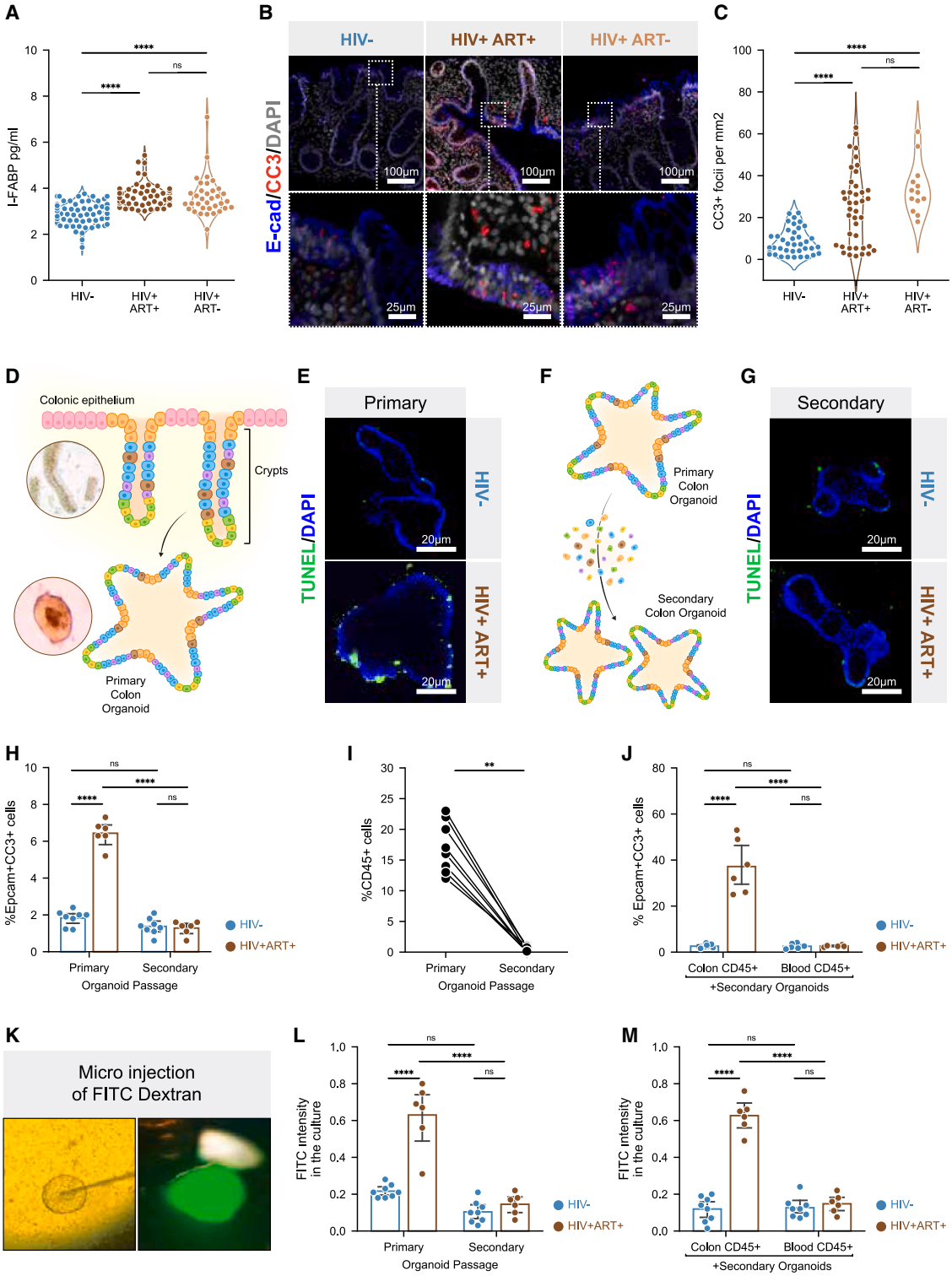

Figure 1. Intestinal barrier disruption in people with HIV (PWH) on antiretroviral therapy (ART) is mediated by colon-resident immune cells

(A) I-FABP concentration in plasma among PWH on ART, PWH without ART, and HIV-uninfected individuals. $n = 100$ (HIV^-), $n = 70$ (HIV^+ART^+), and $n = 35$ (HIV^+ART^-).

(B) Confocal microscopic images of colonic biopsies showing epithelial apoptosis (E-cadherin$^+$ CC3$^+$) among PWH on ART, PWH without ART, and HIV-uninfected individuals. Scale bars, 100 mm (top row); 25 mm (bottom row).

(legend continued on next page)

T cells and epithelial cells. We further demonstrate the importance of PPARs in this process using a murine genetic knockout model and show that PPAR-dependent metabolic dysregulation in colon TRM CD8$^+$ T cells result in epithelial cell apoptosis and impaired barrier integrity.

RESULTS

Intestinal barrier disruption in PWH on ART is mediated by colon-resident immune cells

We observed elevated plasma intestinal fatty-acid-binding protein (I-FABP), a biomarker of intestinal epithelial damage, in PWH who were ART-naive or treated compared with HIV-uninfected individuals (Figure 1A). To examine colon epithelial damage in those with HIV, we stained colonic tissue biopsies for the apoptosis marker cleaved caspase 3 (CC3) and found increased cell death in the epithelium of both ART-naive and ART-treated PWH compared with those without HIV infection (Figures 1B and 1C). Despite these findings, the frequency of intestinal stem cells and proliferative cells in colon crypts remained unchanged with HIV infection (Figures S1A–S1D). We also found no evidence of aberrant tight junctions in PWH on ART using electron tomography of the colon epithelium (Figure S1E). To further assess the mechanism of epithelial apoptosis in PWH, we established a patient-derived colon organoid (“colonoid”) model using endoscopic colon tissue biopsies (Figure 1D). Primary colonoids derived directly *ex vivo* from PWH on ART exhibited greater epithelial apoptosis than those from HIV-uninfected individuals (Figures 1E and S1F). When these colonoids were mechanically dissociated to single cells, epithelial stem cells in the primary colonoids of PWH on ART had the potential to regrow into new colonoids (referred to as “secondary colonoids”) (Figure 1F). This capacity of the intestinal stem cells to form secondary colonoids (“clonogenicity”) was the same between PWH on ART and HIV-uninfected individuals (Figure S1G). Interestingly, the increase in epithelial apoptosis observed in primary colonoids derived from PWH on ART was no longer seen in their secondary colonoids (Figures 1G and 1H). Consistent with this, lactate dehydrogenase (LDH) release, a measure of cellular damage, was increased in primary colonoids from PWH on ART compared with those from HIV-uninfected individuals, but this was not observed in secondary colonoids (Figure S1H). These results indicate that intestinal epithelial cell apoptosis observed *in vivo* was recapitulated in primary colonoids derived from PWH on ART, but this cellular death was lost after disassociation and seeding of secondary colonoids.

To further assess differences in primary and secondary colonoids, we characterized their cellular composition by flow cytometry and identified a loss of CD45$^+$ immune cells in secondary colonoids independent of HIV infection status (Figure 1I). Increased epithelial apoptosis was restored when autologous colon CD45$^+$ immune cells from the lamina propria but not peripheral blood were co-cultured with the secondary colonoids from PWH on ART (Figure S1I, Figure 1J). Addition of autologous colon CD45$^+$ immune cells to secondary organoids derived from HIV-uninfected individuals did not result in epithelial apoptosis (Figure 1J). This was again consistent with observations made examining LDH release (Figure S1J). These findings indicate that colon CD45$^+$ immune cells were necessary and sufficient to induce the epithelial apoptosis observed in colonoids derived from PWH on ART.

To determine whether colon epithelial apoptosis in PWH on ART led to a loss of barrier integrity, FITC-dextran was microinjected into the lumen of primary colonoids to measure leakage into the supernatant (Figure 1K). We observed increased FITC leakage in primary colonoid cultures from PWH on ART compared with those from HIV-uninfected individuals (Figure 1L). FITC leakage was lost in secondary colonoids but could be recapitulated with the addition of autologous colon-resident CD45$^+$ immune cells but not autologous blood-derived CD45$^+$ cells from PWH on ART (Figure 1M). Together, these findings indicate that colon-resident CD45$^+$ immune cells from PWH on ART mediate epithelial cell apoptosis and disruption of barrier integrity.

Colon CD8$^+$ T cells from PWH on ART induce epithelial apoptosis via non-canonical functions

To determine which specific CD45$^+$ immune cell subset mediated epithelial apoptosis, we co-cultured secondary colonoids from PWH on ART with autologous colon CD4$^+$ T cells, CD8$^+$

(C) Quantification of confocal imaging for colonic epithelial apoptosis among PWH on ART, PWH without ART, and HIV-uninfected individuals. n = 40 (HIV$^-$), n = 40 (HIV$^+$ART$^+$), and n = 13 (HIV$^+$ ART$^-$).
(D) Schematic showing primary colonoid establishment.
(E) Increased apoptosis (TUNEL$^+$) in primary colonoids derived from PWH on ART compared with uninfected individuals. Scale bar, 20 mm.
(F) Schematic showing secondary (post passaged) colonoid establishment.
(G) Secondary colonoids from PWH on ART show similar levels of epithelial cell apoptosis (TUNEL$^+$) compared with those from HIV-uninfected individuals. Scale bar, 20 mm.
(H) Quantification of flow cytometric analysis of colonic epithelial apoptosis (Epcam$^+$ CC3$^+$) from primary and secondary colonoid cultures. n = 8 (primary and secondary organoids from HIV$^-$), n = 6 (primary and secondary organoids from HIV$^+$ART$^+$).
(I) Quantification of flow cytometric analysis of CD45$^+$ immune population in primary colonoids vs. secondary colonoid cultures. n = 8 individuals (independent of HIV status).
(J) Quantification of flow cytometric analysis of epithelial apoptosis (Epcam$^+$ CC3$^+$) in the organoid co-cultures when secondary organoids are co-cultured with either autologous colonic CD45$^+$ immune cells or blood-derived CD45$^+$ immune cells. n = 8 (primary and secondary organoids from HIV$^-$), n = 6 (primary and secondary organoids from HIV$^+$ART$^+$).
(K) Microinjection of FITC dextran into the lumen of colonoids.
(L) Increased FITC intensity (arbitrary units) in the media of primary organoid cultures from PWH compared with those from secondary organoids from PWH and HIV-uninfected individuals. n = 8 (primary and secondary organoids from HIV$^-$), n = 6 (primary and secondary organoids from HIV$^+$ART$^+$).
(M) Increased FITC intensity (arbitrary units) in the secondary organoid culture media of colonoids from PWH when co-cultured with autologous CD45$^+$ immune cells. n = 8 (primary and secondary organoids from HIV$^-$), n = 6 (primary and secondary organoids from HIV$^+$ART$^+$).
(A, C, H–J, L, and M) Data shown as mean ± SEM. Each point is one individual. ns, $p > 0.05$; *$p < 0.05$; **$p < 0.01$; ****$p < 0.0001$. Analyzed via one-way ANOVA.

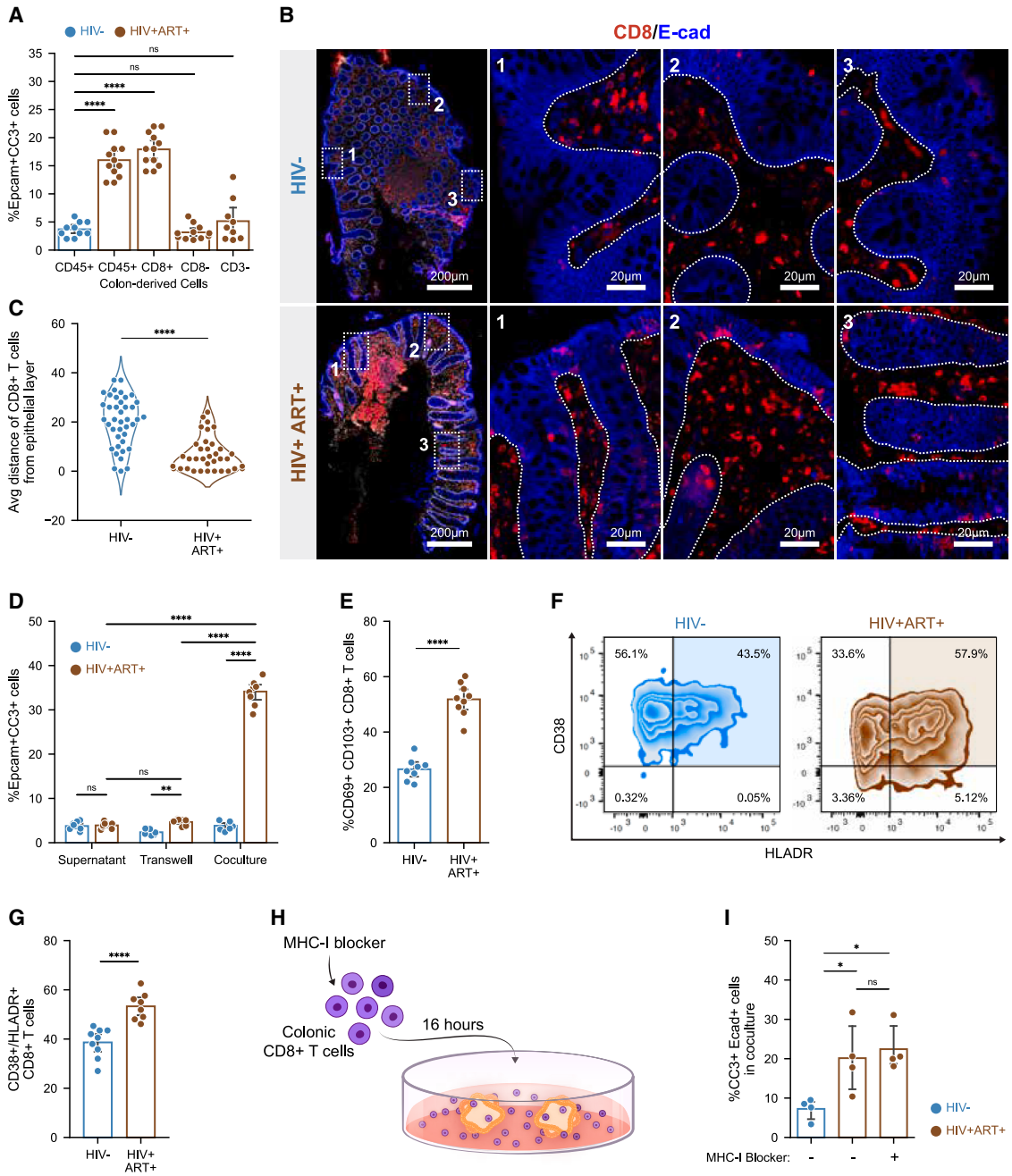

Figure 2. Colonic CD8⁺ T cells from PWH on ART trigger epithelial apoptosis through a contact-dependent, non-canonical mechanism

(A) Flow cytometric quantification of the frequency of apoptotic epithelial cells (Epcam$^+$ CC3$^+$) in co-cultures of secondary colonoids derived from PWH on ART and autologous colonic immune subpopulations. n = 10 (HIV$^-$), n = 12 (HIV$^+$ART$^+$).

(B) Confocal microscopy images of colon biopsy pinches showing the localization of CD8$^+$ T cells relative to the epithelial region. Scale bar, 200 mm; insets, 20 mm.

(C) Quantification of the average distance of CD8$^+$ T cells from the epithelial layer in the colon in PWH on ART and HIV-uninfected individuals. n = 40 (HIV$^-$), n = 40 (HIV$^+$ART$^+$).

(D) Flow cytometric quantification of epithelial apoptosis (Epcam$^+$ CC3$^+$) in colonoids co-cultured with autologous colonic CD8$^+$ T cells in the same well, separated by a transwell or cultured with CD8$^+$ T cell culture supernatants. For transwell assay, n = 10 (HIV$^-$), n = 9 (HIV$^+$ ART$^+$); co-culture setup, n = 9 (HIV-), n = 10 (HIV$^+$ ART$^+$); supernatant culture, n = 8 (HIV-), n = 9 (HIV$^+$ ART$^+$).

(E) Flow cytometric quantification of frequencies of colonic CD69$^+$ CD103$^+$ CD8$^+$ T cell populations (colon TRM CD8$^+$ T cells) in PWH on ART compared with HIV-uninfected individuals. n = 8 (HIV$^-$), n = 9 (HIV$^+$ART$^+$).

(F) Representative flow cytometric plots of colonic CD38$^+$ HLADR$^+$ CD8$^+$ T cells in PWH on ART compared with HIV-uninfected individuals.

(legend continued on next page)

T cells, and non-T immune cells ($CD45^+$ $CD3^-$). Only inclusion of $CD8^+$ T cells recapitulated the epithelial damage observed in primary colonoids (Figure 2A). We then used confocal microscopy to examine the localization of $CD8^+$ T cells relative to the epithelium in colon tissue samples. We found that in PWH on ART, colon $CD8^+$ T cells were localized closer or within the epithelial layer compared with those in people who were HIV-uninfected (Figures 2B, 2C, and S2A). There was no significant difference in the frequency of total $CD8^+$ T cells in the colon between PWH and uninfected individuals (Figure S2B). To better understand how $CD8^+$ T cells were mediating this epithelial apoptosis, we cultured colonoids with autologous $CD8^+$ T cells, either separated by a transwell, or together, or with T cell supernatants. This demonstrated that epithelial apoptosis was primarily dependent on direct contact between $CD8^+$ T cells and epithelial cells, although there may be some contribution from soluble factors (Figure 2D). These findings indicate that close proximity of colon $CD8^+$ T cells to the epithelium is necessary for epithelial apoptosis in PWH on ART.

As TRM $CD8^+$ T cells in the colon play a pivotal role in protection against infections and tumors, we analyzed memory ($CD45RO^+$) and resident ($CD69^+$ $CD103^{+/-}$) subsets and observed that $CD103^+$ TRM ($CD45RO^+$ $CD69^+$ $CD103^+$; hereafter TRM $CD8^+$ T cells) cells were more frequent in PWH on ART than in HIV-uninfected individuals (Figure 2E). However, there was no difference in total memory $CD8^+$ T cells ($CD45RO^+$ $CD8^+$) (Figure S2C). These TRM $CD8^+$ T cells were also more activated ($CD38^+$ HLA^-DR^+) in PWH on ART than HIV-uninfected people (Figures 2F, 2G and S2D). Notably, we found that colon-derived immune cells from PWH on ART had higher levels of intracellular IL-15 compared with uninfected individuals (Figure S2E). This suggests that T cells may be contributing to their own activation because IL-15 can stimulate T cell activation.[20] However, when TRM $CD8^+$ T cells from HIV-uninfected people were activated (by stimulation with phytohemagglutinin [PHA], CD3/CD28 antibody, or IL-15) and co-cultured with secondary colonoids, these cells failed to induce epithelial apoptosis, indicating that T cell activation was not sufficient for this activity (Figure S2F). We additionally found that TRM $CD8^+$ T cells from PWH had reduced effector cytokine (IFNγ and TNFα) and perforin production and no change in granzyme secretion (Figures S2G–S2J). Additionally, blockade of these pathways did not prevent $CD8^+$ T cell-mediated epithelial apoptosis in colonoids from PWH on ART (Figure S2K) and $CD8^+$ T cell-mediated epithelial apoptosis operated independently of MHC-I (Figures 2H and 2I). Overall, we demonstrate that TRM $CD8^+$ T cells from PWH on ART mediate epithelial cell apoptosis through a contact-dependent, non-canonical mechanism.

Colon $CD8^+$ T cells from PWH on ART exhibit impaired lipid metabolism

To further understand functional differences in colon TRM $CD8^+$ T cells from PWH, we performed differential gene expression (DGE) analysis, which demonstrated downregulation of multiple lipid-metabolism-associated genes and pathways in PWH on ART relative to HIV-uninfected individuals (Figures 3A and 3B). Similar findings were observed in DGE analysis of colon TRM $CD8^+$ T cells from an independent South African cohort of PWH (Figure S3A). In both datasets, the peroxisome proliferator-activated receptor γ (*PPARγ*) was downregulated in PWH on ART. We also observed a significant reduction in the expression of genes downstream of PPARγ, such as *CD36*, which encodes a membrane protein that facilitates the uptake of long-chain fatty acids (FAs)[21]; *Dgat2* (diacylglycerol O-acyltransferase 2), an enzyme crucial for triglyceride synthesis[21,22]; *Pnpla7*, which is thought to modulate intracellular lipid droplets (LDs)[23]; and *DGKa* (diacylglycerol kinase alpha) and *DGKg* (diacylglycerol kinase gamma), enzymes that play a central role in LD formation by regulating intracellular diacylglycerol (DAG).[23,24] These genes were identified as PPARγ-regulated based on prior studies demonstrating the presence of PPAR response elements (PPREs) in their promoters.[25] We further confirmed that PPARγ protein expression was downregulated in colon TRM $CD8^+$ T cells from PWH on ART (Figure S3B). Because PPARs are critical FA sensors,[26–28] downregulation of these genes, along with reduced expression of other PPAR family members, highlights the broad disruption in lipid metabolism pathways in colon TRM $CD8^+$ T cells in PWH on ART.

Due to the transcriptional dysregulation of lipid metabolism in colon TRM $CD8^+$ T cells from PWH, we examined the metabolic requirements of these cells. We found that colon TRM $CD8^+$ T cells in HIV-uninfected people were highly dependent upon FA utilization, as demonstrated by reduced mitochondrial oxidative metabolism when incubated with etomoxir, an inhibitor of carnitine palmitoyltransferase-1A (CPT1A), which assists in the shuttling of FA into the mitochondria for fatty acid oxidation (FAO)[29] (Figures 3C and 3D). This was not observed in $CD8^+$ T cells from the periphery of HIV-uninfected individuals (Figure S3C). The mitochondrial oxidative metabolism of colon TRM $CD8^+$ T cells was not affected by the absence of other metabolic substrates such as glucose or glutamine (Figures 3C and 3D). These findings indicate that colon TRM $CD8^+$ T cells are highly dependent upon FAO for their maintenance, unlike their peripheral counterparts.

To further investigate the role of FAO in colon TRM $CD8^+$ T cells, we treated these cells with tritiated palmitic acid and measured the release of tritiated water as an indicator of FAO activity (Figure 3E). Our results demonstrated a reduction of TRM $CD8^+$ T cell FAO in PWH on ART relative to those who were HIV-uninfected (Figure 3F). Treatment of $CD8^+$ T cells from HIV-uninfected individuals with etomoxir also resulted in FAO reduction (Figure 3F). We next examined mitochondrial bioenergetics by measuring basal respiration and spare capacity, which are essential for meeting cellular ATP demand. Colon TRM $CD8^+$ T cells from PWH demonstrated impaired mitochondrial oxidative metabolism, including reduced basal respiration and spare capacity

(G) Quantification of frequencies of colonic $CD38^+$ $HLADR^+$ $CD8^+$ T cells in PWH on ART compared with HIV-uninfected individuals. $n = 9$ (HIV^-), $n = 8$ (HIV^+ART^+).
(H) Schematic showing MHC-I blocking of colonic $CD8^+$ T cells prior to their co-culture with colonoids.
(I) Flow cytometric quantification of frequencies of epithelial apoptotic cells ($Epcam^+$ $CC3^+$) with MHC-I blocking in PWH on ART compared with HIV-uninfected individuals. $n = 4$ per group.
(A, C–E, G, and I) Data shown as mean ± SEM. Each point is one individual. ns, $p > 0.05$; *$p < 0.05$; **$p < 0.01$; ****$p < 0.0001$. Analyzed via one-way ANOVA.

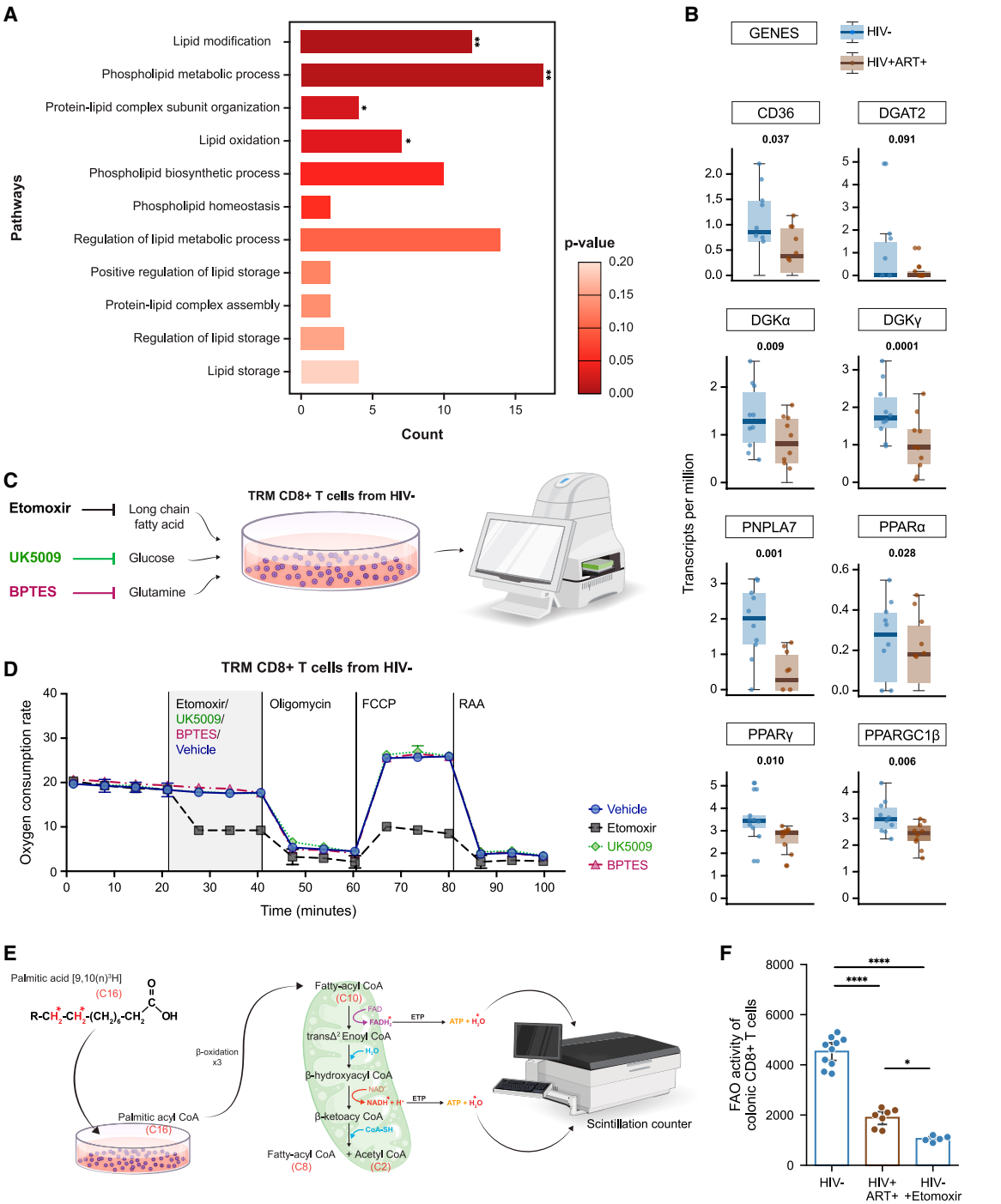

Figure 3. Impaired lipid metabolism in colon TRM CD8$^+$ T cells in PWH on ART

(A) Gene ontology pathway analysis showing gene counts that are enriched in colon TRM CD8$^+$ T cells in PWH compared with those who are HIV-uninfected. Benjamini-Hochberg-corrected p values: *$p < 10^{-2}$, **$p < 10^{-5}$.

(B) Log (transcripts per million) expression of PPARγ downstream target genes integral to lipid droplet (LD) biogenesis in colon TRM CD8$^+$ T cells from HIV-uninfected individuals (blue, $n = 10$) and PWH on ART (brown, $n = 9$).

(C) Schematic of Seahorse substrate oxidation assay used to assess metabolic pathways in colon TRM CD8$^+$ T cells.

(D) Oxygen consumption rate (OCR; pmol/min/cells) of sorted colon TRM CD8$^+$ T cells from HIV-uninfected individuals was measured by Seahorse assay to evaluate their metabolic profile. The OCR was measured during the mitochondrial stress test with the addition of oligomycin, carbonyl cyanide p-trifluoromethoxy phenylhydrazone (FCCP), and rotenone and antimycin A (RAA) drugs. Results were normalized with the cell count. $n = 5$ per group.

(E) Schematic showing assessment of fatty acid oxidation (FAO) by radioactive tracing of tritiated palmitic acid.

(legend continued on next page)

compared with those from HIV-uninfected people (Figures S3D and S3E). Exogenous FA treatment with palmitic acid failed to restore mitochondrial oxidative metabolism in these cells (Figures S3D and S3E). However, colon TRM CD8$^+$ T cells from PWH had similar FA uptake capacity when compared with HIV-uninfected individuals, as indicated by the uptake of labeled palmitic acid (BODIPY C16) (Figures S3F and S3G). These data suggest that colon TRM CD8$^+$ T cells from PWH are highly dependent upon FAO and can uptake FA from their local environment but are not able to efficiently utilize exogenous FA for FAO.

Treatment with a PPARγ agonist restores lipid homeostasis in colon CD8$^+$ T cells from PWH on ART

Intracellular LDs act as an internal lipid reserve that supplies FAs for cellular metabolism. Given the downregulation of the lipid sensor PPARγ and its downstream targets, we explored whether LDs serve as the source of FAs for FAO in colon TRM CD8$^+$ cells. We measured FAO in colon TRM CD8$^+$ T cells from HIV-uninfected individuals after blocking DGAT and ATGL, two key enzymes that are involved in LD biogenesis and lipolysis, respectively (Figure 4A). We demonstrated that blocking these enzymes in colon TRM CD8$^+$ T cells reduced FAO, indicating that these cells mobilize FAs from their LDs for FAO (Figure 4B). We also observed that using DGAT or ATGL (Atglistatin) inhibitors (Figure S4A) to deplete LDs also resulted in colon TRM CD8$^+$ T cells from HIV-uninfected individuals inducing epithelial apoptosis (Figure S4B). This suggests that LD-mobilized FA are crucial for CD8$^+$ T cell-intrinsic FAO and that disrupting LD metabolism in TRM CD8$^+$ T cells lead to epithelial cell apoptosis.

We next stained colon TRM CD8$^+$ T cells for LDs and observed LD depletion in cells from PWH on ART compared with HIV-uninfected individuals (Figures 4C and 4D). This depletion could not be reversed with exogenous FA (palmitic acid) (Figures 4C and 4D), similar to our observation that administration of exogenous FA did not enhance mitochondrial metabolism (Figures S3C and S3D). However, we found that treatment of these cells with the PPARγ agonist rosiglitazone replenished LDs (Figures 4C and 4D). This was consistent with the role of PPARγ in regulating LD biogenesis (Figure 4E). Treatment with rosiglitazone also increased FAO in TRM CD8$^+$ T cells from PWH, whereas the PPARγ antagonist GW9662 significantly reduced FAO in these cells from HIV-uninfected individuals (Figure 4F). These findings demonstrate that colon TRM CD8$^+$ T cells are dependent on LDs to maintain metabolic homeostasis but have depleted LDs and impaired FAO in those infected with HIV on ART. Importantly, this LD depletion and FAO defect could be reversed with the PPARγ agonist rosiglitazone.

Colon TRM CD8$^+$ T cell from PWH on ART mediate epithelial apoptosis through PPARγ-dependent lipid scavenging

Our findings revealed that colon TRM CD8$^+$ T cells from PWH on ART exhibit impaired lipid metabolism. To investigate how this lipid metabolic dysregulation results in epithelial apoptosis, we performed live imaging of TRM CD8$^+$ T cells and colonoids to observe their cellular interactions. We stained colonoid epithelial lipids with DiI, a lipophilic dye that integrates into lipid bilayers, and CellMask, an amphipathic dye that anchors to the plasma membrane through its hydrophilic and lipophilic components. These were co-cultured with autologous TRM CD8$^+$ T cells labeled with CellTrace Violet. We then measured contacts between labeled CD8$^+$ T cells and epithelial cells and demonstrated that TRM CD8$^+$ T cells from PWH had significantly more interactions than those from HIV-uninfected subjects (Figures 5A, 5B and S5A). Additionally, we also observed higher levels of transfer of DiI-labeled epithelial cell lipids to TRM CD8$^+$ T cells from PWH compared with those from HIV-uninfected individuals (Figure 5C). This epithelial lipid transfer to TRM CD8$^+$ T cells was abolished in the presence of the actin polymerization inhibitor latrunculin A or the PI-3Kinase inhibitor wortmannin (Figure 5C). These inhibitors were previously shown to prevent capture of plasma membrane fragments from target cells by T cells and cancer cells.[30,31] Finally, treatment of colon TRM CD8$^+$ T cells with latrunculin A or wortmannin significantly reduced epithelial apoptosis in samples derived from PWH on ART (Figure 5D). To further confirm the lipid scavenging of TRM CD8$^+$ T cells, we co-cultured Cy5-PE-labeled liposomal nanoparticles mimicking plasma membranes (Figure 5E) and showed rapid transfer of Cy5-PE to CD8$^+$ T cells (Figure 5F). These findings suggest that colon TRM CD8$^+$ T cells from PWH on ART contact epithelial cells, acquire lipids from epithelial membranes, and contribute to their apoptosis.

Having shown that restoring PPARγ in colon TRM CD8$^+$ T cells of PWH enhances their FAO activity by replenishing their intrinsic LDs (Figure 4F), we aimed to determine whether treatment with a PPARγ agonist could reverse epithelial apoptosis caused by PPARγ-deficient colon TRM CD8$^+$ T cells. When colon CD8$^+$ T cells from PWH on ART were treated with the PPARγ agonist rosiglitazone (Figure 5G), they induced less epithelial cell death (Figure 5H), decreased CD8$^+$ T cell-epithelial contacts (Figures S5B and S5C), and reduced DiI transfer from the co-cultured epithelial cells (Figure S5D). Additionally, colon TRM CD8$^+$ T cells from HIV-uninfected individuals treated with the PPARγ antagonist GW9662 now induced epithelial apoptosis (Figure 5H), had increased contacts with the epithelial cells (Figures S5E and S5F), and increased DiI transfer from the epithelium (Figure S5G). These results indicate that reduced PPARγ signaling in colon TRM CD8$^+$ T cells results in lipid scavenging from epithelial cells, which induces epithelial cell apoptosis. Importantly, this can be reversed with the PPARγ agonist rosiglitazone.

Colon CD8$^+$ T cell PPAR signaling is required for maintaining intestinal barrier integrity in a murine model

To provide further support that the observed downregulation of PPARs in colon TRM CD8$^+$ T cells in PWH on ART was critical for epithelial apoptosis, we generated a mouse lacking

(F) FAO activity (counts per minute [cpm]) of metabolized ^{3}H-palmitic acid normalized to colon TRM CD8$^+$ T cell count from HIV-uninfected individuals and PWH on ART, accompanied by the FAO activity calculated from 4 mM etomoxir-treated colon TRM CD8$^+$ T cells. n = 10 (HIV$^-$), n = 7 (HIV$^+$ART$^+$), and n = 5 (etomoxir-treated CD8$^+$ T cells from HIV).
(B, D, J) Data shown as mean ± SEM. Each point is one individual.

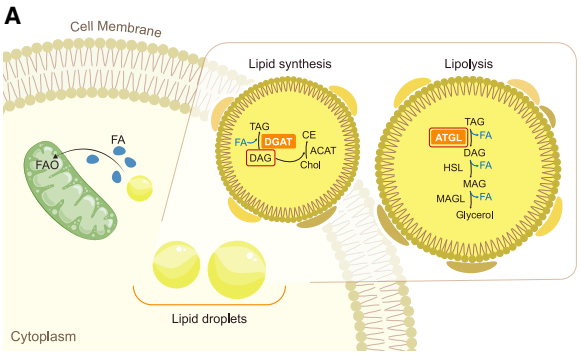

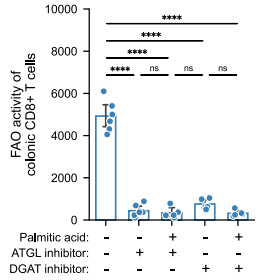

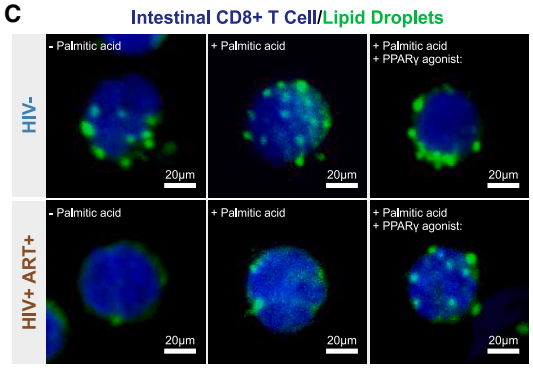

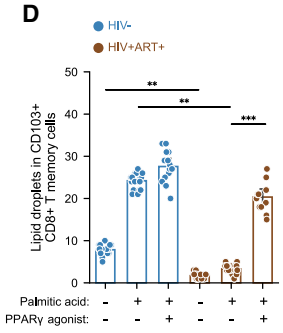

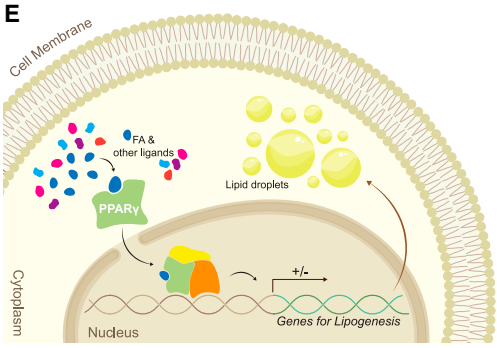

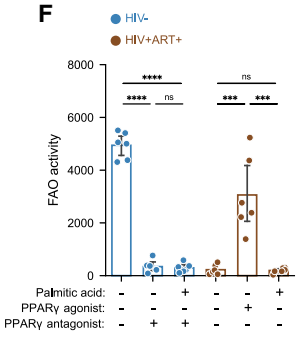

Figure 4. PPARγ-mediated lipid droplet (LD) repletion restores lipid homeostasis in colonic CD8⁺ T cells from PWH on ART

(A) Diagram showing LD biogenesis and lipolysis pathways, with key enzymes highlighted in orange.

(B) Quantification of FAO activity (counts per minute [cpm]) of metabolized ^{3}H-palmitic acid normalized to colon TRM CD8⁺ T cell count from HIV-uninfected individuals upon ATGL inhibition (Atglistatin) to block lipolysis and DGAT inhibition to block LD biogenesis. $n = 6$ per group.

(C) Confocal imaging of LDs (detected with Nile Red staining shown in green) in colon TRM CD8⁺ T cells from PWH on ART and HIV-uninfected individuals with addition of palmitic acid or palmitic acid and PPARγ agonist.

(D) Quantification of LDs in colon TRM CD8⁺ T cells from PWH on ART and HIV-uninfected individuals. $n = 14$ (HIV⁻), $n = 10$ (HIV⁺ART⁺).

(E) Diagram showing how PPARγ ligands and fatty acids (FAs) activate PPAR signaling, which then regulates LD dynamics.

(F) Quantification of FAO activity in colon TRM CD8⁺ T cells from HIV-uninfected individuals and PWH when treated with PPARγ antagonist or PPARγ agonist. $n = 6$ per group.

(B, D, F) Data shown as mean ± SEM. Each point, one individual. ns, $p > 0.05$; *$p < 0.05$; **$p < 0.01$; ****$p < 0.0001$. Analyzed via one-way ANOVA.

PPARα/β/γ (isoforms that are functionally redundant in mice) in CD8⁺ T cells (CD8-PPAR total knockout [TKO]) (Figure S6A). Colon CD8⁺ T cells from the CD8-PPAR TKO mice exhibited LD depletion, consistent with a critical role for PPARs in LD biogenesis (Figures 6A, 6B and S6B). We also observed a significant increase in epithelial cell apoptosis in the colon when TKO CD8⁺ T cells isolated from mesenteric lymph nodes were adoptively transferred into a Rag2 KO mice compared with transfer of wild-type (WT) CD8⁺ T cells (Figure 6C, 6D and 6E). Additionally, higher levels of epithelial apoptosis were observed when mouse colonoids were co-cultures with colonic CD8⁺ T cells from CD8-TKO mice compared with WT mice (Figures S6C and S6D). We next assessed *in vivo* intestinal barrier disruption by giving mice a FITC-dextran enema and showed that Rag2 KO mice that received TKO CD8⁺ T cells had significantly increased barrier disruption compared with those that received WT CD8⁺ T cells (Figure 6F). These findings further support a model in which downregulation of PPAR in colon TRM CD8⁺ T cells results in intestinal epithelial cell apoptosis and intestinal barrier disruption through heterotypic cellular interactions.

DISCUSSION

Colon-resident CD8⁺ T cells predominantly exist as memory populations, with TRM cells being the most prevalent subset.[32] These cells are shaped by the local tissue microenvironment and, unlike circulating memory CD8⁺ T cells, are strategically positioned within the mucosa to continuously survey the epithelium for signs of infection or abnormal cellular behavior.[18] The integrity of the intestinal barrier depends on interactions between tissue-resident CD8⁺ T cells and the epithelium,[33] and disruption of these interactions has been implicated in various diseases, including IBD, where excessive activity of colonic CD8⁺ T cells can compromise the intestinal epithelial barrier.[10,11,34] However, the impact of TRM CD8⁺ T cells on intestinal epithelium in PWH, a population with persistent disruption of intestinal barrier integrity, has not been extensively studied.

Our findings underscore the critical role of interactions between colon TRM CD8⁺ T cells and epithelial cells, demonstrating how metabolic dysregulation of the CD69⁺ CD103⁺ subset significantly compromises epithelial barrier integrity in PWH on ART. These colon-resident CD8⁺ T cells directly mediate

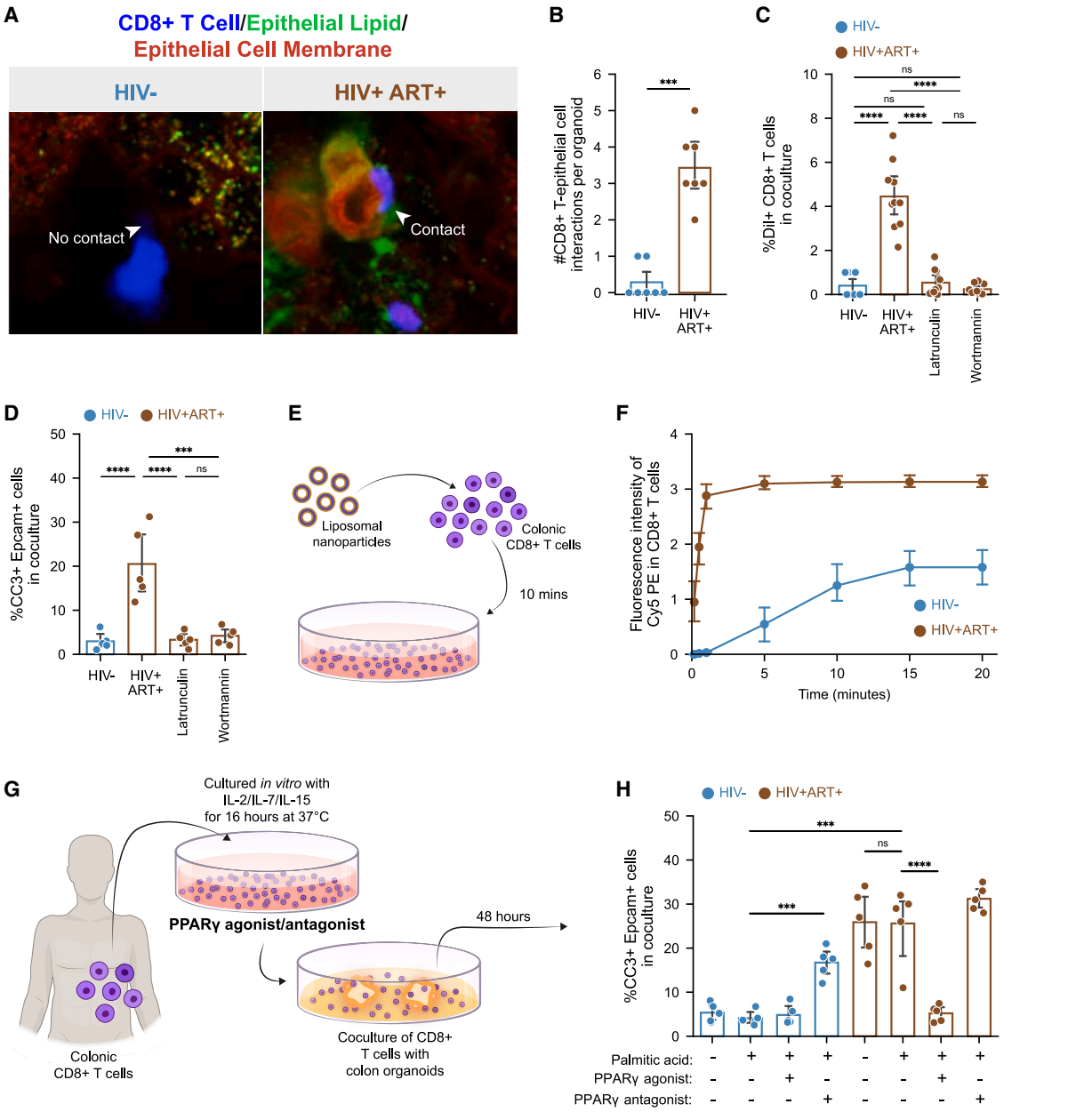

Figure 5. PPARγ agonist treatment of TRM CD8⁺ T cells from PWH abrogates T cell-mediated epithelial apoptosis

(A) Snapshots from time-lapse live imaging comparing colon TRM CD8⁺ T cell from PWH and HIV-uninfected individuals when co-cultured with autologous secondary colonoids demonstrating proximity and interaction of colon TRM CD8⁺ T cells (blue) with epithelial cells (red) and epithelial lipids (DiI in green).

(B) Quantification of the frequency of colon TRM CD8⁺ T cells interacting with the epithelial cells in organoid co-cultures. $n = 7$ per group.

(C) Quantification of the frequency of DiI⁺ colon TRM CD8⁺ T cells from colonoid co-cultures. Experiments were also performed with treatment with an inhibitor of actin polymerization (latrunculin) and phosphatidylinositol 3-kinase (PI3K; wortmannin). $n = 6$ (HIV^-), $n = 10$ (HIV^+ART^+).

(D) Flow cytometric quantification of epithelial apoptosis ($Epcam^+$ $CC3^+$) in co-cultures when colonic CD8⁺ T cells were treated with latrunculin or wortmannin. $n = 5$ per group.

(E) Schematic showing colon TRM CD8⁺ T cells co-cultured with fluorophore-tagged liposomal nanoparticles.

(F) Quantification of liposomal nanoparticle fluorescence in colon TRM CD8⁺ T cells following co-cultre. $n = 5$ per group.

(G) Schematic showing colon TRM CD8⁺ T cell treated with PPARγ antagonist or agonist and then co-cultured with autologous secondary colonoids.

(H) Flow cytometric quantification of epithelial apoptosis ($Epcam^+$ $CC3^+$) in TRM CD8⁺ T cell co-cultures treated with PPARγ agonist or antagonist. $n = 5$ per group.

(B–D, F, H) Data shown as mean ± SEM. Each point is one individual. ns, $p > 0.05$; *$p < 0.05$; **$p < 0.01$; ****$p < 0.0001$. Analyzed via one-way ANOVA.

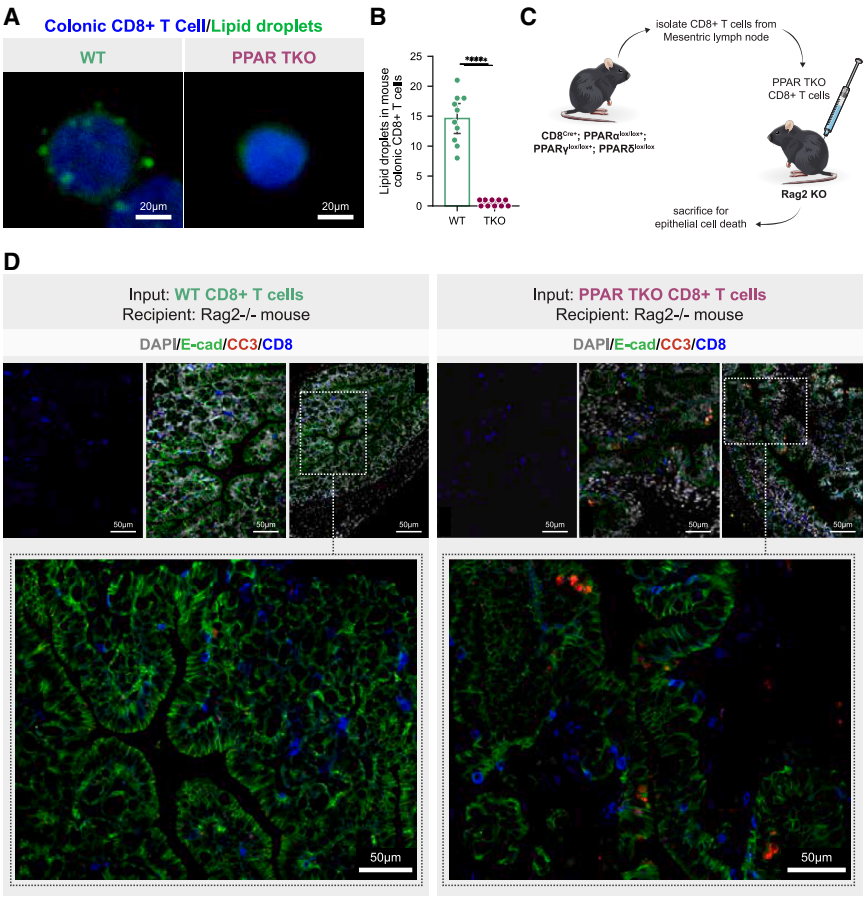

Figure 6. PPARγ signaling in colonic CD8⁺ T cells is critical for maintaining intestinal barrier integrity

(A) Confocal imaging of lipid droplets (LDs; green) in colonic CD8⁺ T cells from WT and CD8⁺ T cell from PPAR TKO mice. Scale bar, 20 mm.

(B) Quantification of LDs in colonic CD8⁺ T cells from WT and PPAR TKO mice. $n = 10$ per group.

(C) Schematic showing isolation of CD8⁺ T cells from the mesenteric lymph node of PPARα$^{-/-}$, PPARδ$^{lox/lox}$, PPARγ$^{lox/lox}$; CD8-cre mice that were then adoptively transferred into Rag2$^{-/-}$ mice via tail vein injection.

(D) Confocal imaging of colon mucosa of Rag2$^{-/-}$ mice showing epithelial apoptosis (DAPI⁺ E-cadherin⁺ CC3⁺) when CD8⁺ T cells (DAPI⁺ CD8⁺) from PPARα$^{-/-}$, PPARδ$^{lox/lox}$, PPARγ$^{lox/lox}$; CD8-cre mice were adoptively transferred into Rag2$^{-/-}$ mice via tail vein injection compared with transfer of WT CD8⁺ T cells. Scale bar, 100 mm; inset, 50 mm.

(E) Quantification of epithelial apoptosis in recipient Rag2$^{-/-}$ when CD8⁺ T cells from PPARα$^{-/-}$, PPARδ$^{lox/lox}$, PPARγ$^{lox/lox}$; CD8-cre mice were adoptively transferred into Rag2$^{-/-}$ mice via tail vein injection compared with transfer of WT CD8⁺ T cells. $n = 7$ per group.

(F) Quantification of FITC dextran in peripheral blood as a measure of intestinal barrier disruption of recipient Rag2$^{-/-}$ when CD8⁺ T cells from PPARα$^{-/-}$, PPARδ$^{lox/lox}$, PPARγ$^{lox/lox}$; CD8-cre mice were adoptively transferred into Rag2$^{-/-}$ mice via tail vein injection compared with transfer of WT CD8⁺ T cells. $n = 7$ per group.

(B, E, F) Data shown as mean ± SEM. Each point is one mouse. ns, $p > 0.05$; *$p < 0.05$; **$p < 0.01$; ****$p < 0.0001$. Analyzed via t test.

epithelial apoptosis, leading to disruption of the intestinal barrier. The observed lack of intestinal stem cell proliferation in colon crypts during epithelial apoptosis suggests insufficient compensatory mechanisms to restore homeostasis. Additionally, in PWH, apoptotic epithelial cells may accumulate within the epithelium, failing to provide necessary proliferative cues to the stem cell compartment, thereby contributing to a sustained loss of epithelial barrier integrity.

Although chronic T cell activation is known to drive epithelial damage in cancer and IBD, previous reports have attributed this to mechanisms such as epithelial tight junction remodeling or cytokine-mediated injury.[35,36] However, our findings suggest that in PWH, epithelial damage necessitates direct contact with CD8⁺ T cells and may involve non-canonical CD8⁺ T cell behavior. This points to previously unrecognized mechanisms of colon TRM CD8⁺ T cell dysfunction during HIV infection, with broader implications for understanding immune-epithelial interactions in both infectious and non-infectious chronic inflammatory diseases.

The immunometabolic properties of CD8⁺ T cells significantly contribute to the maintenance of systemic homeostasis in PWH,[37,38] but the role of tissue-resident CD8⁺ T cells is incompletely understood. In the skin, tissue-resident CD8⁺ T cells have an increased need for FA metabolism for their function and survival.[39] We discovered that colon TRM CD8⁺ T cells depend on FAO for homeostasis in a similar manner. We showed that, in PWH on ART, colon TRM CD8⁺ T cells exhibit a reduction in their intrinsic lipid reserves due to decreased PPARγ signaling, similar to other reports of the central role of PPARs in LD biogenesis and FAO.[23–25] Importantly, our transgenic mouse models with PPAR depletion specifically in CD8⁺ T cells reveal that T cell metabolic dysregulation can independently influence epithelial homeostasis beyond the context of HIV.

PPARs are crucial lipid sensors with distinct roles in lipid metabolism.[26] Specifically, PPARγ acts as a key transcriptional regulator governing intracellular lipid processing, storage, and utilization.[25] Notably, PPARγ-responsive elements (PPREs) are present in the proximal regions of key genes involved in LD

formation and FAO, including CD36 and DGAT,[25–28] suggesting a transcriptional regulation mechanism underlying these metabolic alterations. In line with this, our findings show that when PPARγ expression is reduced, the ability of cells to efficiently store lipids in LDs is impaired because critical downstream targets involved in LD formation, such as DGAT1, are not adequately expressed. Our findings show that colon TRM CD8$^+$ T cells in PWH, despite decreased PPARγ expression, continue to uptake FAs but fail to convert them into LDs effectively. Pharmacological activation of PPARγ restores gene expression critical for LD biogenesis and stabilizes intracellular lipid homeostasis, enabling regulated lipid storage. These observations suggest that dampened PPARγ activity disrupts the processing and storage of lipids rather than their uptake. FA uptake may occur via compensatory mechanisms that allow lipid uptake independent of traditional lipid scavenger receptors such as CD36.[40] Although CD36 is a key transporter for FA uptake, emerging evidence suggests that lipid acquisition can also occur through alternative pathways, such as the palmitoylation of plasma membrane proteins, which facilitates lipid trafficking and membrane remodeling. Palmitoylation, a post-translational modification involving the addition of palmitic acid to proteins, has been shown to enhance the localization of key signaling molecules to lipid rafts, enabling efficient lipid internalization.[41,42] This mechanism provides a potential route for FA uptake in CD8$^+$ T cells, allowing lipid incorporation into cellular membranes despite the downregulation of classical transporters.

To determine whether impaired LD formation results from altered metabolic pathways (e.g., increased FAO, ER stress, or dysregulated lipid trafficking), further studies are required. Additionally, to compensate for reduced lipid reserves, TRM CD8$^+$ T cells scavenge lipids from the plasma membranes of adjacent epithelial cells. Although this lipid transfer supports T cell metabolic homeostasis, it causes epithelial cell damage, apoptosis, and ultimately compromises the epithelial barrier.

The role of PPARγ as a transcriptional regulator of T cell function and fate has been previously proposed, with evidence indicating that PPARδ (a functionally close isoform of PPARγ) ablation enhances effector functions in CD8$^+$ T cells.[42,43] This suggests that PPARγ downregulation in colon TRM CD8$^+$ T cells may contribute to their hyperactivation and cytotoxicity toward its target cells. Furthermore, activating PPARγ could unintentionally impact other immune cells essential for mucosal barrier integrity, particularly Th17 cells.[44,45] Given the pivotal role of Th17 cells in epithelial homeostasis, the potential adverse effects of PPARγ-targeted therapies warrant careful consideration. Comprehensive profiling of PPARα/β/γ protein expression in various immune and epithelial cells from colon biopsies could further clarify the roles of these nuclear receptors in intestinal immunity.

Environmental factors, such as ART, diet, lipid metabolism, and microbiome changes, may also impact PPARγ regulation in TRM CD8$^+$ T cells. ART has been linked to metabolic disruptions that could enhance PPARγ downregulation. Additionally, dietary lipids and microbial metabolites might further modulate PPARγ transcription. Further research is required to clarify how these elements contribute to metabolic and immune disturbances in PWH.

Our study highlights the importance of PPAR-linked metabolic regulation of TRM CD8$^+$ T cells in understanding the interactions between immune cells and epithelial cells. However, further studies are needed to determine the mechanism of PPAR downregulation during HIV infection. PPAR downregulation is not exclusive to HIV; it has also been reported in inflammatory conditions like IBD, colitis, and aging.[46–48] The shared feature across these conditions is chronic inflammation, indicating that PPAR signaling may broadly influence immune regulation in various inflammatory disorders. Additionally, the specific ways in which intestinal CD8$^+$ T cells adapt to metabolic demands during HIV infection or chronic inflammation merit further investigation. Tumor cells maintain their survival and proliferation in nutrient-poor conditions by scavenging extracellular protein and lipids from adjacent cells.[49–51] Similarly, immune cells are known to feed off other cells through trogocytosis, the transfer of plasma membrane fragments from one cell to another.[51,52] Trogocytosis may be particularly important in the colon, where CD8$^+$ T cells are highly activated and maintain elevated states of metabolic demand.[53] Employing state-of-the-art heterotypic co-culture organoid assays, we characterized how colon-resident CD8$^+$ T cells acquire lipids from adjacent epithelial plasma membranes. However, the specific mechanistic details of this lipid transfer, and the pathways of lipid utilization, require further study. Additionally, although we demonstrated that treatment with rosiglitazone, a PPARγ agonist and approved drug for the management of metabolic syndrome, can restore lipid homeostasis and mitigate epithelial apoptosis in our *ex vivo* models, the therapeutic potential of this approach in humans remains to be assessed.

In summary, we found that PWH have persistent intestinal epithelial damage, evidenced by elevated plasma I-FABP levels in both ART-naive and -treated individuals. Consistent with this, colonic biopsies showed increased epithelial apoptosis in PWH, despite unchanged intestinal stem cell frequencies. This epithelial cell apoptosis was recapitulated in a colon organoid model derived from patient biopsies and was dependent upon co-culture with autologous colon TRM CD8$^+$ T cells. These cells exhibited downregulation of PPARs and lipid metabolism pathways and impaired FAO. Further, genetic ablation of PPARs in CD8$^+$ T cells in a mouse model emphasized the important role of these lipid regulators in maintaining epithelial-immune circuits and gut barrier function more broadly, not just in the context of HIV infection. Importantly, treatment of TRM CD8$^+$ T cells from PWH with the PPARγ agonist rosiglitazone restored lipid homeostasis and ameliorated CD8$^+$ T cell-induced epithelial apoptosis. These findings may lead to the development of therapies to help improve intestinal barrier integrity and combat the associated comorbidities in PWH as well as other diseases that impact intestinal homeostasis.

Limitations of the study

Our findings suggest that metabolic dysregulation in TRM CD8$^+$ T cells contributes to epithelial apoptosis and barrier disruption, however, the precise molecular mechanisms underlying these interactions remain unclear. Although we demonstrated that TRM CD8$^+$ T cells acquire lipids from epithelial cells, the pathways facilitating lipid transfer—such as trogocytosis or extracellular vesicle exchange—require further investigation.

Additionally, our study identifies a link between PPARγ downregulation, lipid scavenging by $CD8^+$ T cells, and epithelial apoptosis, but a comprehensive understanding of how diet, ART, and microbiome changes influence this metabolic landscape remains necessary. Furthermore, given that PPARγ downregulation also occurs in other inflammatory conditions like IBD, colitis, and aging, it is essential to explore whether our observations reflect a broader immunometabolic phenomenon common across multiple chronic inflammatory diseases.

RESOURCE AVAILABILITY

Lead contact

Further information and requests for resources and reagents should be directed to, and will be fulfilled by, the lead contact, Douglas S. Kwon (dkwon@mgh.harvard.edu).

Materials availability

All unique/stable reagents directly used in this study are available from the lead contact with a completed materials transfer agreement.

Data and code availability

- Human colon-resident $CD8^+$ T cell bulk RNA sequencing (RNA-seq) has been deposited in the Gene Expression Omnibus (GEO) repository under the accession number GEO: GSE299833.
- Microscopy data reported in this paper will be shared by the lead contact upon request.
- Any additional information required to reanalyze the data reported in this paper is available from the lead contact upon request.

ACKNOWLEDGMENTS

We thank the study participants for donation of clinical samples, Daniel Worrall and the Ragon Institute Clinical Team for clinical study support, and the study participants and Michael Waring for flow cytometry assistance. We also thank Zeynep Ertüz and Meilin Zhu for assistance with illustration and figure refinement, respectively. U.D.A. was supported by the NIH grant no. 1K99DK136365; D.S.K., O.H.Y., and H.N.K. were supported by the NIH grant no. 1R01DK126545; D.S.K., O.H.Y., and U.D.A. were supported by the NIH grant no. 1R01DK133919.

AUTHOR CONTRIBUTIONS

Conceptualization: U.D.A., O.H.Y., A.E.R., and D.S.K.; investigation: U.D.A., L.M.F., A.N.P., H.B., P.S., and A.H.; generation of liposomal nanoparticles: B.K. and B.R.; microscopic imaging assistance: T.J.D.; electron tomography: M.L. and P.B.; RNA-seq analysis: Q.Z., S.N., and A.S.; procurement of clinical specimens: O.A., F.M., S.K., and H.K.; writing – original draft: U.D.A.; writing – review and editing: D.S.K., O.H.Y., and other authors.

DECLARATION OF INTERESTS

The authors declare no competing interests.

STAR★METHODS

Detailed methods are provided in the online version of this paper and include the following:

Received: October 24, 2024
Revised: April 10, 2025
Accepted: August 14, 2025
Published: September 11, 2025

REFERENCES

1. Somsouk, M., Estes, J.D., Deleage, C., Dunham, R.M., Albright, R., Inadomi, J.M., Martin, J.N., Deeks, S.G., McCune, J.M., and Hunt, P.W. (2015). Gut epithelial barrier and systemic inflammation during chronic HIV infection. AIDS *29*, 43–51. https://doi.org/10.1097/QAD.0000000000000511.
2. Brenchley, J.M., Price, D.A., and Douek, D.C. (2006). HIV disease: fallout from a mucosal catastrophe? Nat. Immunol. *7*, 235–239. https://doi.org/10.1038/ni1316.
3. Lerner, A.M., Eisinger, R.W., and Fauci, A.S. (2020). Comorbidities in Persons With HIV: The Lingering Challenge. JAMA *323*, 19–20. https://doi.org/10.1001/jama.2019.19775.
4. Brenchley, J.M., Price, D.A., Schacker, T.W., Asher, T.E., Silvestri, G., Rao, S., Kazzaz, Z., Bornstein, E., Lambotte, O., Altmann, D., et al. (2006). Microbial translocation is a cause of systemic immune activation in chronic HIV infection. Nat. Med. *12*, 1365–1371. https://doi.org/10.1038/nm1511.
5. Hiltensperger, M., Kumar, V., Zegarra-Ruiz, D., Dehner, C., Khan, N., Costa, F.R.C., Tiniakou, E., Greiling, T., Ruff, W., Barbieri, A., et al. (2018). Erratum for the Report "Translocation of a gut pathobiont drives autoimmunity in mice and humans" by S. Manfredo Vieira. Science *360*, eaat9922. https://doi.org/10.1126/science.aat9922.
6. Manfredo Vieira, S., Hiltensperger, M., Kumar, V., Zegarra-Ruiz, D., Dehner, C., Khan, N., Costa, F.R.C., Tiniakou, E., Greiling, T., Ruff, W., et al. (2018). Translocation of a gut pathobiont drives autoimmunity in mice and humans. Science *359*, 1156–1161. https://doi.org/10.1126/science.aar7201.
7. Tanes, C., Walker, E.M., Slisarenko, N., Gerrets, G.L., Grasperge, B.F., Qin, X., Jazwinski, S.M., Bushman, F.D., Bittinger, K., and Rout, N. (2021). Gut Microbiome Changes Associated with Epithelial Barrier Damage and Systemic Inflammation during Antiretroviral Therapy of Chronic SIV Infection. Viruses *13*, 1567. https://doi.org/10.3390/v13081567.
8. Sandler, N.G., and Douek, D.C. (2012). Microbial translocation in HIV infection: causes, consequences and treatment opportunities. Nat. Rev. Microbiol. *10*, 655–666. https://doi.org/10.1038/nrmicro2848.
9. Sim, J.H., Mukerji, S.S., Russo, S.C., and Lo, J. (2021). Gastrointestinal Dysfunction and HIV Comorbidities. Curr. HIV/AIDS Rep. *18*, 57–62. https://doi.org/10.1007/s11904-020-00537-8.

10. Lerner, A.M., Eisinger, R.W., and Fauci, A.S. (2020). Comorbidities in Persons With HIV: The Lingering Challenge. JAMA *323*, 19–20. https://doi.org/10.1001/jama.2019.19775.

11. Smit, M., Cassidy, R., Cozzi-Lepri, A., Quiros-Roldan, E., Girardi, E., Mammone, A., Antinori, A., Saracino, A., Bai, F., Rusconi, S., et al. (2017). Projections of non-communicable disease and health care costs among HIV-positive persons in Italy and the U.S.A.: A modelling study. PLOS One *12*, e0186638. https://doi.org/10.1371/journal.pone.0186638.

12. Alzahrani, J., Hussain, T., Simar, D., Palchaudhuri, R., Abdel-Mohsen, M., Crowe, S.M., Mbogo, G.W., and Palmer, C.S. (2019). Inflammatory and immunometabolic consequences of gut dysfunction in HIV: Parallels with IBD and implications for reservoir persistence and non-AIDS comorbidities. EBioMedicine *46*, 522–531. https://doi.org/10.1016/j.ebiom.2019.07.027.

13. Müller, S., Lory, J., Corazza, N., Griffiths, G.M., Z'graggen, K., Mazzucchelli, L., Kappeler, A., and Mueller, C. (1998). Activated CD4+ and CD8+ cytotoxic cells are present in increased numbers in the intestinal mucosa from patients with active inflammatory bowel disease. Am. J. Pathol. *152*, 261–268.

14. Allaire, J.M., Crowley, S.M., Law, H.T., Chang, S.-Y., Ko, H.-J., and Vallance, B.A. (2018). The Intestinal Epithelium: Central Coordinator of Mucosal Immunity: (Trends in Immunology 39, 677–696, 2018). Trends Immunol. *39*, 677–696. https://doi.org/10.1016/j.it.2018.04.002.

15. Degirmenci, B., Valenta, T., Dimitrieva, S., Hausmann, G., and Basler, K. (2018). GLI1-expressing mesenchymal cells form the essential Wnt-secreting niche for colon stem cells. Nature *558*, 449–453. https://doi.org/10.1038/s41586-018-0190-3.

16. Biton, M., Haber, A.L., Rogel, N., Burgin, G., Beyaz, S., Schnell, A., Ashenberg, O., Su, C.-W., Smillie, C., Shekhar, K., et al. (2018). T Helper Cell Cytokines Modulate Intestinal Stem Cell Renewal and Differentiation. Cell *175*, 1307–1320.e22. https://doi.org/10.1016/j.cell.2018.10.008.

17. Shoshkes-Carmel, M., Wang, Y.J., Wangensteen, K.J., Tóth, B., Kondo, A., Massasa, E.E., Itzkovitz, S., and Kaestner, K.H. (2018). Subepithelial telocytes are an important source of Wnts that supports intestinal crypts. Nature *557*, 242–246. https://doi.org/10.1038/s41586-018-0084-4.

18. Hoytema van Konijnenburg, D.P., Reis, B.S., Pedicord, V.A., Farache, J., Victora, G.D., and Mucida, D. (2017). Intestinal Epithelial and Intraepithelial T Cell Crosstalk Mediates a Dynamic Response to Infection. Cell *171*, 783–794.e13. https://doi.org/10.1016/j.cell.2017.08.046.

19. Agudo, J., Park, E.S., Rose, S.A., Alibo, E., Sweeney, R., Dhainaut, M., Kobayashi, K.S., Sachidanandam, R., Baccarini, A., Merad, M., et al. (2018). Quiescent Tissue Stem Cells Evade Immune Surveillance. Immunity *48*, 271–285.e5. https://doi.org/10.1016/j.immuni.2018.02.001.

20. Schenkel, J.M., Fraser, K.A., Casey, K.A., Beura, L.K., Pauken, K.E., Vezys, V., and Masopust, D. (2016). IL-15-Independent Maintenance of Tissue-Resident and Boosted Effector Memory CD8 T Cells. J. Immunol. *196*, 3920–3926. https://doi.org/10.4049/jimmunol.1502337.

21. Hao, J.-W., Wang, J., Guo, H., Zhao, Y.-Y., Sun, H.-H., Li, Y.-F., Lai, X.-Y., Zhao, N., Wang, X., Xie, C., et al. (2020). CD36 facilitates fatty acid uptake by dynamic palmitoylation-regulated endocytosis. Nat. Commun. *11*, 4765. https://doi.org/10.1038/s41467-020-18565-8.

22. Yen, C.-L.E., Stone, S.J., Koliwad, S., Harris, C., and Farese, R.V., Jr. (2008). Thematic review series: glycerolipids. DGAT enzymes and triacylglycerol biosynthesis. J. Lipid Res. *49*, 2283–2301. Thematic Review Series. https://doi.org/10.1194/jlr.R800018-JLR200.

23. Chang, P., Sun, T., Heier, C., Gao, H., Xu, H., and Huang, F. (2020). Interaction of the Lysophospholipase PNPLA7 with Lipid Droplets through the Catalytic Region. Mol. Cells *43*, 286–297. https://doi.org/10.14348/molcells.2020.2283.

24. Krishna, S., and Zhong, X.-P. (2013). Regulation of Lipid Signaling by Diacylglycerol Kinases during T Cell Development and Function. Front. Immunol. *4*, 178. https://doi.org/10.3389/fimmu.2013.00178.

25. Costa, V., Gallo, M.A., Letizia, F., Aprile, M., Casamassimi, A., and Ciccodicola, A. (2010). PPARG: Gene Expression Regulation and Next-Generation Sequencing for Unsolved Issues. PPAR Res. *2010*, 409168. https://doi.org/10.1155/2010/409168.

26. Poulsen, Ll., Siersbæk, M., and Mandrup, S. (2012). PPARs: fatty acid sensors controlling metabolism. Semin. Cell Dev. Biol. *23*, 631–639. https://doi.org/10.1016/j.semcdb.2012.01.003.

27. Nagy, L., Tontonoz, P., Alvarez, J.G., Chen, H., and Evans, R.M. (1998). Oxidized LDL regulates macrophage gene expression through ligand activation of PPARgamma. Cell *93*, 229–240. https://doi.org/10.1016/s0092-8674(00)81574-3.

28. Varga, T., Czimmerer, Z., and Nagy, L. (2011). PPARs are a unique set of fatty acid regulated transcription factors controlling both lipid metabolism and inflammation. Biochim. Biophys. Acta *1812*, 1007–1022. https://doi.org/10.1016/j.bbadis.2011.02.014.

29. Buck, M.D., O'Sullivan, D., Klein Geltink, R.I., Curtis, J.D., Chang, C.-H., Sanin, D.E., Qiu, J., Kretz, O., Braas, D., van der Windt, G.J.W., et al. (2016). Mitochondrial Dynamics Controls T Cell Fate through Metabolic Programming. Cell *166*, 63–76. https://doi.org/10.1016/j.cell.2016.05.035.

30. Aucher, A., Magdeleine, E., Joly, E., and Hudrisier, D. (2008). Capture of plasma membrane fragments from target cells by trogocytosis requires signaling in T cells but not in B cells. Blood *111*, 5621–5628. https://doi.org/10.1182/blood-2008-01-134155.

31. Shin, J.H., Jeong, J., Maher, S.E., Lee, H.-W., Lim, J., and Bothwell, A.L.M. (2021). Colon cancer cells acquire immune regulatory molecules from tumor-infiltrating lymphocytes by trogocytosis. Proc. Natl. Acad. Sci. USA *118*, e2110241118. https://doi.org/10.1073/pnas.2110241118.

32. Mackay, L.K., Rahimpour, A., Ma, J.Z., Collins, N., Stock, A.T., Hafon, M.-L., Vega-Ramos, J., Lauzurica, P., Mueller, S.N., Stefanovic, T., et al. (2013). The developmental pathway for CD103(+)CD8+ tissue-resident memory T cells of skin. Nat. Immunol. *14*, 1294–1301. https://doi.org/10.1038/ni.2744.

33. Konjar, Š., Ferreira, C., Blankenhaus, B., and Veldhoen, M. (2017). Intestinal Barrier Interactions with Specialized CD8 T Cells. Front. Immunol. *8*, 1281. https://doi.org/10.3389/fimmu.2017.01281.

34. Le, N.T.T., Mazahery, C., Nguyen, K., and Levine, A.D. (2021). Regulation of Intestinal Epithelial Barrier and Immune Function by Activated T Cells. Cell. Mol. Gastroenterol. Hepatol. *11*, 55–76. https://doi.org/10.1016/j.jcmgh.2020.07.004.

35. Wang, F., Graham, W.V., Wang, Y., Witkowski, E.D., Schwarz, B.T., and Turner, J.R. (2005). Interferon-gamma and tumor necrosis factor-alpha synergize to induce intestinal epithelial barrier dysfunction by up-regulating myosin light chain kinase expression. Am. J. Pathol. *166*, 409–419. https://doi.org/10.1016/s0002-9440(10)62264-x.

36. Klatt, N.R., Harris, L.D., Vinton, C.L., Sung, H., Briant, J.A., Tabb, B., Morcock, D., McGinty, J.W., Lifson, J.D., Lafont, B.A., et al. (2010). Compromised gastrointestinal integrity in pigtail macaques is associated with increased microbial translocation, immune activation, and IL-17 production in the absence of SIV infection. Mucosal Immunol. *3*, 387–398. https://doi.org/10.1038/mi.2010.14.

37. Sáez-Cirión, A., and Sereti, I. (2021). Immunometabolism and HIV-1 pathogenesis: food for thought. Nat. Rev. Immunol. *21*, 5–19. https://doi.org/10.1038/s41577-020-0381-7.

38. Crakes, K.R., Santos Rocha, C., Grishina, I., Hirao, L.A., Napoli, E., Gaulke, C.A., Fenton, A., Datta, S., Arredondo, J., et al. (2019). PPARα-targeted mitochondrial bioenergetics mediate repair of intestinal barriers at the host-microbe intersection during SIV infection. Proc. Natl. Acad. Sci. USA. *116*, 24819–24829. https://doi.org/10.1073/pnas.1908977116.

39. Pan, Y., Tian, T., Park, C.O., Lofftus, S.Y., Mei, S., Liu, X., Luo, C., O'Malley, J.T., Gehad, A., Teague, J.E., et al. (2017). Survival of tissue-resident memory T cells requires exogenous lipid uptake and metabolism. Nature *543*, 252–256. https://doi.org/10.1038/nature21379.

40. Schwenk, R.W., Holloway, G.P., Luiken, J.J.F.P., Bonen, A., and Glatz, J.F.C. (2010). Fatty acid transport across the cell membrane: regulation

by fatty acid transporters. Prostaglandins Leukot. Essent. Fatty Acids *82*, 149–154. https://doi.org/10.1016/j.plefa.2010.02.029.

41. Bijlmakers, M.-J., and Marsh, M. (2003). The on-off story of protein palmitoylation. Trends Cell Biol. *13*, 32–42. https://doi.org/10.1016/s0962-8924(02)00008-9.
42. Chamberlain, L.H., and Shipston, M.J. (2015). The physiology of protein S-acylation. Physiol. Rev. *95*, 341–376. https://doi.org/10.1152/physrev.00032.2014.
43. Cen, B., Wei, J., Wang, D., and DuBois, R.N. (2024). Peroxisome Proliferator-Activated Receptor δ Suppresses the Cytotoxicity of CD8+ T Cells by Inhibiting RelA DNA-Binding Activity. Cancer Res Commun. *4*, 2673–2684. https://doi.org/10.1158/2767-9764.CRC-24-0264.
44. Planas, D., Fert, A., Zhang, Y., Goulet, J.-P., Richard, J., Finzi, A., Ruiz, M. J., Marchand, L.R., Chatterjee, D., Chen, H., et al. (2020). Pharmacological Inhibition of PPARγ Boosts HIV Reactivation and Th17 Effector Functions, While Preventing Progeny Virion Release and de Infection. Pathog. Immun. *5*, 177–239. https://doi.org/10.20411/pai.v5i1.348.
45. Klotz, L., Burgdorf, S., Dani, I., Saijo, K., Flossdorf, J., Hucke, S., Alferink, J., Nowak, N., Beyer, M., Mayer, G., et al. (2009). The nuclear receptor PPAR gamma selectively inhibits Th17 differentiation in a T cell-intrinsic fashion and suppresses CNS autoimmunity. J. Exp. Med. *206*, 2079–2089. https://doi.org/10.1084/jem.20082771.
46. Dou, X., Xiao, J., Jin, Z., and Zheng, P. (2015). Peroxisome proliferator-activated receptor-γ is downregulated in ulcerative colitis and is involved in experimental colitis-associated neoplasia. Oncol. Lett. *10*, 1259–1266. https://doi.org/10.3892/ol.2015.3397.
47. Wang, M., Yan, Y., Zhang, Z., Yao, X., Duan, X., Jiang, Z., An, J., Zheng, P., Han, Y., Wu, H., et al. (2021). Programmed PPAR-α downregulation induces inflammaging by suppressing fatty acid catabolism in monocytes. iScience *24*, 102766. https://doi.org/10.1016/j.isci.2021.102766.
48. Motawi, T.K., Shaker, O.G., Ismail, M.F., and Sayed, N.H. (2017). Peroxisome Proliferator-Activated Receptor Gamma in Obesity and Colorectal Cancer: the Role of Epigenetics. Sci. Rep. *7*, 10714. https://doi.org/10.1038/s41598-017-11180-6.
49. Zhang, Y., Kurupati, R., Liu, L., Zhou, X.Y., Zhang, G., Hudaihed, A., Filisio, F., Giles-Davis, W., Xu, X., Karakousis, G.C., et al. (2017). Enhancing CD8 T Cell Fatty Acid Catabolism within a Metabolically Challenging Tumor Microenvironment Increases the Efficacy of Melanoma Immunotherapy. Cancer Cell *32*, 377–391.e9. https://doi.org/10.1016/j.ccell.2017.08.004.
50. Kamphorst, J.J., Nofal, M., Commisso, C., Hackett, S.R., Lu, W., Grabocka, E., Vander Heiden, M.G., Miller, G., Drebin, J.A., Bar-Sagi, D., et al. (2015). Human pancreatic cancer tumors are nutrient poor and tumor cells actively scavenge extracellular protein. Cancer Res. *75*, 544–553. https://doi.org/10.1158/0008-5472.CAN-14-2211.
51. Michalopoulou, E., Bulusu, V., and Kamphorst, J.J. (2016). Metabolic scavenging by cancer cells: when the going gets tough, the tough keep eating. Br. J. Cancer *115*, 635–640. https://doi.org/10.1038/bjc.2016.256.
52. Joly, E., and Hudrisier, D. (2003). What is trogocytosis and what is its purpose? Nat. Immunol. *4*, 815. https://doi.org/10.1038/ni0903-815.
53. Konjar, Š., and Veldhoen, M. (2019). Dynamic Metabolic State of Tissue Resident CD8 T Cells. Front. Immunol. *10*, 1683. https://doi.org/10.3389/fimmu.2019.01683.
54. Das Adhikari, U., Eng, G., Farcasanu, M., Avena, L.E., Choudhary, M.C., Triant, V.A., Flagg, M., Schiff, A.E., Gomez, I., Froehle, L.M., et al. (2022). Fecal Severe Acute Respiratory Syndrome Coronavirus 2 (SARS-Cov-2) RNA Is Associated With Decreased Coronavirus Disease 2019 (COVID-19) Survival. Clin. Infect. Dis. *74*, 1081–1084. https://doi.org/10.1093/cid/ciab623.
55. Trapecar, M., Khan, S., Roan, N.R., Chen, T.-H., Telwatte, S., Deswal, M., Pao, M., Somsouk, M., Deeks, S.G., Hunt, P.W., et al. (2017). An Optimized and Validated Method for Isolation and Characterization of Lymphocytes from HIV+ Human Gut Biopsies. AIDS Res. Hum. Retrovir. *33*, S31–S39. https://doi.org/10.1089/AID.2017.0208.
56. Morgenstern, Y., Das Adhikari, U., Ayyash, M., Elyada, E., Tóth, B., Moor, A., Itzkovitz, S., and Ben-Neriah, Y. (2017). Casein kinase 1-epsilon or 1-delta required for Wnt-mediated intestinal stem cell maintenance. EMBO J. *36*, 3046–3061. https://doi.org/10.15252/embj.201696253.

STAR★METHODS

KEY RESOURCES TABLE

REAGENT or RESOURCE	SOURCE	IDENTIFIER
Antibodies		
Rabit monoclonal anti-Cleaved Caspase-3 (Asp175)	Cell Signaling Technology	Cat# 9661
Goat polyclonal anti-E-Cadherin	bio-techne	Cat# AF748; RRID: AB_355568
Rat monoclonal anti-CD8 (KT15)	ThermoFisher Scientific	Cat# MA5-16761; RRID: AB_2538244
Anti-goat Secondary antibody	Invitrogen	Cat# A11055; RRID: AB_2534102
Anti-goat Secondary antibody	Invitrogen	Cat# A11057; RRID: AB_2534104
Anti-rabbit Secondary antibody	Invitrogen	Cat# A11034; RRID: AB_2576217
Anti-rabbit Secondary antibody	Invitrogen	Cat# A11034; RRID: AB_2576217
Anti-rat Secondary antibody	Invitrogen	Cat# A21208; RRID: AB_2535794
Human Olfactomedian 4	Cell Signaling Technology	Cat#14369
Rabit polyclonal anti-Ki67	BioCare	Cat# CRM325B
Anti-human CD45 (HI30) BV605	BD Biosciences	Cat# 564047; RRID: AB_2744403
Anti-human CD3 (UCHT1) BV711	BD Biosciences	Cat# 563725; RRID: AB_2744392
Anti-human CD3 (UCHT1) PerCP/Cyanine5.5	BioLegend	Cat# 300430; RRID: AB_893299
Anti-human CD4 (RPA-T4) BUV395	BD Biosciences	Cat# 564724; RRID: AB_2738917
Anti-human CD8 (RPA-T8) BUV395	BD Biosciences	Cat# 563795; RRID: AB_2722501
Anti-human CD8 (SK1) APC-H7	BD Biosciences	Cat# 560179; RRID: AB_1645481
Anti-human CD8 (SK1) V500	BD Biosciences	Cat# 561617; RRID: AB_10896281
Anti-human CD45RO (UCHL1) PE	BioLegend	Cat# 304206; RRID: AB_2564160
Anti-human CD69 (FN50) BV750	BD Biosciences	Cat# 747522; RRID: AB_2872182
Anti-human CD103 (Ber-ACT8) PE/Cyanine7	BioLegend	Cat# 350212; RRID: AB_2561598
Anti-human CD38 (HIT2) AF700	BioLegend	Cat# 303524; RRID: AB_303524
Anti-human CD38 (HIT2) BV711	BioLegend	Cat# 563965; RRIC:AB_2738516
Anti-human HLA-DR (L234) BV785	BioLegend	Cat# 307642; RRID: AB_2563461
Anti-human IFN-g (B27) PE-CF594	BD Biosciences	Cat# 562392; RRID: AB_11153859
Anti-human TNF-a (MAb11) FITC	BioLegend	Cat# 502906; RRID: AB_315258
Anti-human TNF-a (MAb11) BV785	BD Biosciences	Cat# 502948; RRID: AB_2565858
Anti-human Perforin (dG9) BV711	BioLegend	Cat# 308130; RRID: AB_2687190
Anti-human Perforin (B-D48) PerCP/Cyanine5.5	BD Biosciences	Cat# 353314; RRID: AB_2571971
Anti-human Perforin (B-D48) BV421	BioLegend	Cat# 353314; RRID: AB_11149688
Anti-human Granzyme B (GB11) BV421	BD Biosciences	Cat# 563389; RRID: AB_2738175
Anti-human Granzyme B (QA16A02) PerCP/ Cyanine5.5	BioLegend	Cat# 372212; RRID: AB_2728378
Rabit monoclonal anti-Cleaved Caspase-3 (Asp175) PE-Cy7	Cell Signaling Technologies	Cat# 64772S
Rabit monoclonal anti-Cleaved Caspase-3 AF488	Bio-techne	Cat# IC835G; RRID: AB_2728840
Anti-human CD326/EpCam (EBA-1) BV421	BD Biosciences	Cat# 563180; RRID: AB_2738050
Anti-human CD324/E-Cadherin (DECMA-1) BV421	BioLegend	Cat# 147319; RRID: AB_2750483
Anti-mouse CD326/EpCam (G8.8) APC	Invitrogen	Cat# 17-5791-82; RRID: AB_2716944
Mouse monoclonal anti-CD107a (LAMP-1)	eBioscience	Cat# 14-1079-80; RRID: AB_467426
Biological samples		
Human colon biopsies and peripheral blood from healthy patients	This paper	N/A
Human colon biopsies and peripheral blood from HIV+, ART- patients	This paper	N/A

(*Continued on next page*)

Continued

REAGENT or RESOURCE	SOURCE	IDENTIFIER
Human colon biopsies and peripheral blood from HIV+, ART+ patients	This paper	N/A
Chemicals, peptides, and recombinant proteins		
DAPI	ThermoFisher Scientific	Cat# 62248
NucBlue™ Fixed Cell ReadyProbes™ Reagent (DAPI)	ThermoFisher Scientific	Cat# R37606
Piperacillin-tazobactam (Zosyn)	Massachusetts General Hospital Pharmacy	N/A
Amphotericin B	Sigma Aldrich	Cat# 15290-026
Penicillin Streptomycin	Gibco	Cat# 15070-063
HEPES	Sigma Aldrich	Cat# H3375
L-glutamine	Sigma Aldrich	Cat# 25030-081
RPMI Medium	Thermo Fisher Scientific	Cat# 21870092
Matrigel	Corning	Cat# 356255
TrypLE™ Express Enzyme	Thermo Fisher Scientific	Cat# 12604013
L-WRN Conditioned Media	This paper	N/A
Advanced DMEM/F-12	Gibco	Cat# 12634010
Fetal bovine serum	Cytvia	Cat# SH30071
GlutaMAX™	Gibco	Cat# 35050061
RSPO-1	Thermo/PeproTech	Cat# 120-38
B27	Gibco	Cat# 17504044
Nicotinamide	Sigma-Aldrich	Cat# 72340
EGF	PeproTech	Cat# AF-100-15
A83-01	Cayman Chemical	Cat# 9001799
SB202190	Cayman Chemical	Cat# 10010399
Y-27632	Cayman Chemical	Cat# 10005583
EDTA	Invitrogen	Cat# 15575-038
DTT (dithiothreitol)	Thermo Fisher Scientific	Cat# R0861
Collagenase	Worthington Biochem	Cat# LS005273
DNase I	Millipore Sigma	Cat# 11284932001
Liberase™ TM	Millipore Sigma	Cat# 5401119001
Fluorescein isothiocyanate–dextran (FITC)	Millipore Sigma	Cat# 60842-46-8
MHC-I blocker	ThermoFisher Scientific	Cat# H463; clone W6/32
Phytohemagglutinin (PHA)	ThermoFisher Scientific	Cat# 00-4977-93
Human IL-15	PeproTech	Cat# 200-15
Emapulimab	Med Chem. Express	Cat# HY-P99191
GranzB inhibitor	Sigma	Cat# 368050
Etenercept	Med Chem. Express	Cat# HY-108847
ConcanamycinA	Sigma	Cat# C9705
FASL Blocker	Sigma	Cat# 341291
Tritiated palmitic acid	This paper	N/A
BSA	ThermoFisher Scientific	ThermoFisher Scientific
Palmitic Acid	Pekin Elmer	Cat# NET043001MC
BODIPY C16	ThermoFisher Scientific	Cat# D3821
ATGL Inhibitor (Atglistatin 15284)	Cayman Chemicals	Cat# NC0663866
DGAT inhibitor (AZD 3988)	Tocris	Cat# 483710
PPARg agonist (rosiglitazone)	Tocris	Cat# 5325
PPARg antagonist (GW9662)	Tocris	Cat# 1508
Nile Red	Cayman Chemicals	Cat# 30787

(*Continued on next page*)

Continued

REAGENT or RESOURCE	SOURCE	IDENTIFIER
Human IL-2	StemCell Technologies	Cat# 78036
Human IL-7	Peprotech/Thermo	Cat# 200-07
Vybrant™ DiI Cell-Labeling Solution	ThermoFisher Scientific	Cat# V22885
Cell Mask	ThermoFisher Scientific	Cat# C10045
CellTrace™ Violet Cell Proliferation Kit	ThermoFisher Scientific	Cat# C34571
Latrunculin A	ThermoFisher Scientific	Cat# L12370
Wortmannin	ThermoFisher Scientific	Cat# 603-042
Cy5-PE-labeled liposomal nanoparticles (18:1 Cyanine 5 PE)	Avanti Research	Cat# 810335
DPBS	Corning	Cat# MT20031CV
DMSO	ThermoFisher Scientific	Cat# BP231
Paraformaldehyde (PFA)	Electron Microscopy Sciences	Cat# 157-4
Goat Serum	Gibco	Cat# 16210064
Antibody Diluent	Dako	Cat# S0809
Triton-X	Sigma Aldrich	Cat# X100
Hank's Balanced Salt Solution	Gibco	Cat# 14025092
Histopaque®-1077 Hybri-Max™	ThermoFisher Scientific	Cat# H8889
CD45 Microbeads	Miltenyi Biotech	Cat# 130-045-801
Fc Block	BioLegend	Cat# 422302
UltraComp Beads	Invitrogen	Cat# 01-3333-42
GolgiStop™	BD Biosciences	Cat# 554724
ArC™ Amine Reactive Compensation Bead	ThermoFisher Scientific	Cat# A10346
Brefeldin A	Millipore Sigma	Cat# B5936
LIVE/DEAD™ Fixable Blue Dead Cell Stain Kit	ThermoFisher Scientific	Cat# L34962
FACS™ Permeabilizing Solution 2	BD Biosciences	Cat# 347692
Formalin	Sigma Aldrich	Cat# HT501128
Histo-Clear	National Diagnostics	Cat# HS-200
Decloacker	BioCare Medical	Cat# BD1000MM
Tween-20	Sigma Aldrich	Cat# P6585
Tris-buffered saline (TBS)	ThermoFisher Scientific	Cat# NC1660550
ProLong Gold Antifade	ThermoFisher Scientific	Cat# P36980
BSA (fatty acid free)	Sigma Aldrich	Cat# A6003
Palmitic Acid-[9,10-3H]	Pekin Elmer	Cat# NET043001MC
Dowex®1X8 resin	Sigma Aldrich	Cat# 217425
EcoLume	MP Biomedicals	Cat# 882470
RLT Lysis Buffer	Qiagen	Cat#79216
2-mercaptoethanol	Sigma Aldrich	Cat# 63689
Agencourt RNAClean XP SPRI beads	Beckman Coulter	Cat# A63987
Agencourt AMPure XP SPRI Beads	Beckman Coulter	Cat# A63880
Poly-D-Lysine	Gibco	Cat# A3890401
1,2-dioleoyl-sn-glycero-3-phosphocholine	Avanti	Cat# 850375
Cholesterol	Avanti	Cat# 700100
1,2-dioleoyl-sn-glycero-3-phosphoethanolamine-N-(Cyanine 5)	Avanti	Cat# 810335
Antibiotic/Antimycotic	Gibco	Cat# 15240062
Noggin	PeproTech	Cat# 120-10C

(*Continued on next page*)

Continued

REAGENT or RESOURCE	SOURCE	IDENTIFIER
Critical commercial assays		
Seahorse XFp Cell Mito Stress Test	Agilent	Cat# 103010-100
Seahorse XF RPMI assay medium pack, pH 7.4	Agilent	Cat# 103681-100
Seahorse XF Calibrant Solution	Agilent	Cat# 103059-000
Seahorse XFp Cell Culture Miniplates	Agilent	Cat# 103025-100
EasySep™ Mouse CD45 Positive Selection Kit	StemCell Technologies	Cat# 18945
EasySep™ Mouse $CD8^+$ T Cell Isolation Kit	StemCell Technologies	Cat# 19853
EasySep™ Human $CD8^+$ T Cell Isolation Kit	StemCell Technologies	Cat# 17953
Human FABP2/I-FABP DuoSet ELISA	Bio techne	Cat# DY3078
LDH Assay Kit	Abcam	Cat# ab65393
Qubit dsDNA HS Assay Kit	Life Technologies	Cat# Q32851
Nextera XT DNA Library Preparation Kit	Illumina	Cat# FC-131-1024
KAPA Library Quantification kit	Roche Biosystems	Cat# 50-196-5234
Deposited data		
Human colon resident $CD8^+$ T cell bulk RNA-Seq	Gene Expression Omnibus (GEO) repository	GSE299833
Experimental models: Cell lines		
Human: colon organoid	This paper	N/A
Mouse: colon organoid	This paper	N/A
Cultrex HA-R-Spondin1-Fc 293T Cells	R&D Systems	Cat# 3710-001-01
LEADING LIGHT® Wnt Reporter Cell Line	Enzo	Cat# ENZ-61002
Experimental models: Organisms/strains		
C57BL/6J Mice	Jackson Labs	Stock# 000664
Ppara−/− 129S4/SvJae-Pparatm1Gonz/J Mice	Jackson Labs	Stock# 003580
Ppargfl/fl B6.129-Ppargtm2Rev/J Mice	Jackson Labs	Stock# 004584
Ppardfl/fl B6.129S4-Ppardtm1Rev/J Mice	Jackson Labs	Stock# 005897
Cd8a-cre (C57BL/6-Tg(Cd8a-cre)1Itan/J Mice	Jackson Labs	Stock# 008766
Rag2-/-mice	Jackson Labs	Stock# 008449
Software and algorithms		
FlowJo 10.9.0	BD	https://www.flowjo.com/
DESeq2 Package (v1.18.1)	Bioconductor	https://bioconductor.org/packages/release/bioc/html/DESeq2.html
Piano Package (v1.18.1)	Väremo et al. 2013	https://varemo.github.io/piano/
GSEA Package (v3)	N/A	https://www.gsea-msigdb.org/gsea/doc/GSEAUserGuideFrame.html
BioRender	BioRender	https://www.biorender.com/
Other		
ibidi μ-Dish (35 mm, low format)	ibidi	Cat#80136
6 well plate	Corning	Cat#353046
BD Vacutainer® Specialty Tubes	BD	Cat# 364606
300um Pluristrainer	ThermoFisher Scientific	Cat# 43-50300-03
16g blunt-end needles	StemCell Technologies	Cat# 28110
70um cell strainer	ThermoFisher Scientific	Cat# 08-771-2
40um cell strainer	ThermoFisher Scientific	Cat# 352340
12 well plate	Corning	Cat#3512
Nucleocounter Via1-Cassette™	Chemometec	Cat# NC1420193
8-chambered slides	Ibidi	Cat# 80841
FACS Tubes	Falcon	Cat# 352054

(*Continued on next page*)

Continued

REAGENT or RESOURCE	SOURCE	IDENTIFIER
Pressure Cooker	BioCare Medical	Cat# DC2012
Scintillation Counter	Beckman Coulter	Cat# LS6500

EXPERIMENTAL MODEL AND STUDY PARTICIPANT DETAILS

Human subjects

We recruited 20 healthy, HIV-uninfected individuals and 20 people with HIV (PWH) on antiretroviral therapy (ART) for lower endoscopy (colonoscopy). This study (protocol number 2007p002102) was approved by the Massachusetts General Hospital (MGH) institutional review board (IRB), with informed consent obtained in writing after discussion with MGH clinical research coordinators and study physicians. The recruitment criteria for PWH on ART was those with plasma viral load below limit of detection (< 20 copies/mL) for >1 year prior to colonoscopy on ART. Average ART treatment time was a median of 7 years. Healthy participants were recruited to closely match enrolled PWH based on age and sex. Participants were in the age range of 45–57 years old. The study included both male and female participants, with no statistically significant phenotypic differences observed between sexes. Individuals with a history of GI disease, clinical findings from a prior endoscopy, or reported current or prior GI symptoms were excluded.

Sample collection from human subjects

During colonoscopy, pinch biopsies were taken from the transverse colon and placed directly into collection media on ice in the endoscopy suite. Immediately prior to colonoscopy, blood was collected in acid citrate dextrose (ACD) vacutainers (Beckton Dickinson) to isolate PBMCs and plasma (see below for details).

For Figure 1A, we used plasma from previously recruited participants and for Figure 1B and C, we used historically preserved formalin fixed, paraffin embedded (FFPE) biopsy pinches collected under the same protocol.

Epithelial cell isolation

Pinch biopsies were collected in RPMI medium (ThermoFisher Scientific) with 250μg/mL piperacillin-tazobactam (MGH Pharmacy), 2.5 μg/mL amphotericin B (Sigma Aldrich), 100 U/mL penicillin (Gibco), 100 U/mL streptomycin (Gibco), 10 mM HEPES (Sigma Aldrich), 10% Fecal Bovine Serum (FBS, Cytvia) and 2mM L-glutamine (Sigma Aldrich). Pinches were processed immediately, starting with washing with cold phosphate-buffered saline (PBS) and then incubated with 10mM ethylenediaminetetraacetic acid (EDTA, Invitrogen) for 30 min in conical tubes rotated in a 37°C incubator with 5% CO2.

Organoid culture

Organoids were prepared from crypts isolated from biopsy pinches as described before.[54] Isolated crypts were centrifuged at 100g for 3 min. The crypts were embedded in Matrigel (Corning) and incubated at 37°C for 20 min. The media formulation listed below was applied to the solidified Matrigel plugs. For subsequent passaging, the Matrigel plugs were mechanically dissociated by pipetting and exposed to TrypLE (Thermo Fischer Scientific) for 3 min, centrifuged, and resuspended in Matrigel. Media for the organoids was based on L-WRN cell conditioned media (L-WRN CM). Briefly, L-WRN CM was generated by collecting 8 days of supernatant from L-WRN cells, grown in Advanced DMEM/F12 (Gibco) supplemented with 20% FBS, 2 mM GlutaMAX (Gibco), 100 U/mL of penicillin, 100 μg/mL of streptomycin, and 0.25 μg/mL amphotericin. L-WRN CM was diluted 1:1 in Advanced DMEM/F12 and supplemented with additional RSPO-1 conditioned media (10% v/v), generated using Cultrex HA-R-spondin1-Fc 293T cells (R&D Systems). Wnt activity of the conditioned media was assessed and normalized between batches via luciferase reporter activity of TCF/LEF activation (Enzo Leading Light Wnt reporter cell line). Advanced DMEM/F12 was supplemented with 250 μg/mL piperacillin-tazobactam (MGH Pharmacy), 2.5 μg/mL amphotericin B, 100 U/mLpenicillin, 100 U/mL streptomycin, 10mM HEPES, 10% FBS and 2 mM L-glutamine. The following compounds were also added to the growth media: 1X B27 (Gibco), 10 uM nicotinamide (Sigma Aldrich), 50 ng/mL EGF (Novus Biologicals), 500 nM A83-01 (Cayman Chemical), 10 uM SB202190 (Cayman Chemical), and 500 nM PGE2 (Cayman Chemical). 10 uM Y-27632 (Cayman Chemical) was added to crypts only on their initial isolation.

Peripheral blood mononuclear cell (PBMC) isolation

PBMCs were isolated from the blood of HIV-uninfected and -infected individuals by density gradient centrifugation. Blood was transferred to a 50 mL conical and centrifuged at 2600 rpm for 15 min. The resultant plasma layer was stored for later use or discarded. The remainder of the material was brought up to 30 mL volume with Hank's balanced salt solution (HBSS, Gibco). This mixture was then layered with 15 mL of Histopaque-1077 (ThermoFisher Scientific), after which the conical was spun at 1500 rpm for 45 min at room temperature. The PBMC layer was then collected in a new tube, washed twice with HBSS, counted, and frozen in FBS with 10% DMSO solution (ThermoFisher Scientific). PBMCs were cultured in complete RPMI media (10% FBS) in the presence of 50 IU/mL human IL-2 (StemCell Technologies), 10 ng/mL human IL-7 (Pepro Tech), and 10 ng/mL human IL-15 (Pepro Tech). After 48 hours, cells were harvested for co-culture with colonoids or processed for flow cytometry.

Colonic immune cell isolation

Lymphocytes were isolated from intestinal biopsy pinches by modifying the protocol as described.[54,55] Biopsy pinches were transferred to a 50mL conical containing intraepithelial lymphocyte (IEL) stripping buffer (PBS, 10 mM DTT, 5 mM EDTA, 10 mM HEPES, and 5% FCS) and incubated under continuous rotation for 20 min at 37°C. After separating tissue pieces from the supernatant, the tissue was again treated with IEL buffer and incubated while the supernatant was spun down and IELs collected. This process was repeated until all IELs had been isolated from the digested biopsy tissue. Following IEL isolation, biopsy pinches were placed into a collagenase digestion solution. Tissue pinches were incubated in collagenase (Worthington Biochem) at 37°C for 1 hour to release lamina propria (LP) cells. These cells, in combination with isolated IELs, were enriched for CD45+ cells by positive immunomagnetic selection using Miltenyi CD45 microbeads. Cells were cultured in complete RPMI media (10% FBS) in the presence of 50 IU/mL human IL-2, 10 ng/mL human IL-7, and 10 ng/mL human IL-15. After 48 hours, cells were harvested for co-culture with colonoids or processed by flow cytometry.

Colonoid-immune cell co-culture

Immune cells and colonoids were mixed in a ratio of 100,000 immune cells to 20 colonoids and embedded in 70% matrigel and 30% PBS per well in a 24 well plate and cultured with complete colonoid media and IL-7, IL-15 and IL-2. For the transwell setup, 100,000 immune cells were plated per well in complete RPMI media at the bottom chamber of a 24-well transwell system, while the colonoids were embedded in Matrigel and seeded in the transwell insert. For live imaging, colonoids were dyed with Cell MaskRed (ThermoFisher Scientific) labeling the plasma membrane and DiI (ThermoFisher Scientific) labeling the epithelial lipids for 60 min at 37°C. $CD8^+$ T cells were stained with CellTrace Violet (ThermoFisher Scientific) for 30 min at 37°C. Then 100,000 dyed $CD8^+$ T cells were mixed with 20 dyed organoids and embedded in 70ul of matrigel per well and colonoid media was added. Then live cell imaging was performed on the Discoverer7 Zeiss LSM900 confocal microscope at 37°C and with CO2. A z-stack was acquired every 5 min for 18 hours.

Mice

Mice were under the husbandry care of the Department of Comparative Medicine in the Koch Institute for Integrative Cancer Research. All procedures were conducted in accordance with the American Association for Accreditation of Laboratory Animal Care and approved by the Massachusetts Institute of Technology Committee on Animal Care. The following strains were obtained from the Jackson Laboratory: PPARδ fl/fl (B6.129S4-Ppardtm1Rev/J, stock number 005897), PPARγ fl/fl (B6.129-Ppargtm2Rev/J, stock number 004584), $PPAR\alpha^{-/-}$ (129S4/SvJae-Pparatm1Gonz/J, stock number 003580) and CD8cre (C57BL/6-Tg(Cd8a-cre) 1Itan/J, stock number 008766). These mice were bred to obtain CD8-cre/PPARα/δ/γ TKO mice. All mice provided food ad libitum. For experiments, 8 weeks mice, both male and females were used.

CD8+ T cells adoptive transfer

The $CD8^+$ T cells were isolated from the WT and PPAR TKO mice mesenteric lymph nodes using flow cytometric sorting. The isolated WT or PPAR TKO $CD8^+$ T cells were transplanted into 8-week-old $Rag2^{-/-}$ mice (100K cells per mice) through intravenous tail vein injection. Mice were sacrificed 3 weeks post transplantation to obtain colons for analysis.

Crypt isolation from murine colon and murine colonoid culture

Colon crypts were isolated from wild-type C57BL/6 mice as described previously.[56] Briefly, colons were washed with PBS, minced into approximately 1cm segments, and incubated in 8 mM EDTA for 45 min at 37°C. After incubation, EDTA was replaced with PBS and epithelial crypts were obtained by vigorous shaking. The cell suspension was passed through a 70mm filter. Crypts were resuspended in the appropriate volume of one-third primary culture media and two-thirds Matrigel (growth factor reduced, phenol red-free, Corning). Ten microliter droplets of crypts were plated in 48-well tissue culture treated plates (Genesee Scientific). Matrigel was allowed to solidify for 30 min at 37°C, after which 0.5mL of primary culture media was applied. Primary colonoids (crypt-derived) were cultured in advanced DMEM/F12 supplemented with 10% FBS, Antibiotic/Antimycotic (Gibco), GlutaMAX, 1X B-27, 50 ng/mL EGF (PeproTech), 10 mM Y-27632 (StemCell Technologies), 1% Noggin-conditioned medium, and 2% R-spondin1-conditioned media (“primary culture media”). Colonoids were cultured for at least 3 days at 37°C in a humidified, sterile incubator with 5% CO2.

METHOD DETAILS

Immunofluorescence staining of colonoids

Colonoids were cultured on tissue culture-treated cover glass in 8-chambered slides (Ibidi). Colonoids were washed in PBS, then fixed in 4% paraformaldehyde (PFA, Electron Microscopy Sciences) in PBS for 30 min at room temperature. After fixation, cells were washed twice in PBS and then permeabilized for 15 min at room temperature using 0.1% Triton X-100 (Sigma Aldrich). Colonoids were again washed twice with PBS. Protein blocking was done with 5% goat serum in PBS for 1 hour at room temperature. Serum was removed, and organoids were incubated with primary antibodies diluted in antibody diluent (Dako) overnight at 4°C. The following antibodies were used in 1:100 dilution: E cadherin, Muc2, CC3 and Ki67 (see Materials Table for details of the antibodies). After primary antibody incubation, colonoids were washed five times in PBS for 5 min each at room temperature and

then incubated with fluorophore conjugated secondary antibodies (1:300, ThermoFisher Scientific) diluted in 5% goat serum for 3 hours at room temperature. Colonoids were washed five times in PBS for 5 min each at room temperature. TUNEL staining was performed to measure cell death in the colonoids culture according to the manufacturer protocol (ThermoFisher Scientific). To visualize nuclei, colonoids were stained with NucBlue fixed cell reagent (ThermoFisher Scientific) for 10 min at room temperature. Organoids were washed one time in PBS and then imaged on a Zeiss Cell Discoverer LSM900 confocal microscope.

LDH assay for organoid culture

LDH release was measured from colonoids culture media according to the manufacturer's protocol (Abcam).

ELISA

The concentration of I-FABP was measured by ELISA using the Human FABP2/I-FABP DuoSet ELISA kit (R&D Systems), per manufacturer instructions.

FITC dextran microinjection and leakage assays

To perform intraluminal microinjection of FITC-dextran, we selected organoids with a clearly visible, round central lumen to optimize injection efficiency. Twenty organoids were embedded in 20 μl of Matrigel and plated at the center of an ibidi μ-Dish (35 mm, low format; see STAR Methods). On day 3 post-seeding, 0.4 nl of 0.8% fluorescein-conjugated 70 kDa dextran (FITC-Dextran, ThermoFisher Scientific) was injected into the organoid lumen using a micromanipulator (M-152, Narishige, Japan) and a microinjector (MINJ-D, Tritech Research). Injections were performed under a fluorescent inverted stereomicroscope (Zeiss). After injection, organoids were incubated in fresh media for 18–20 hours to allow recovery. To evaluate barrier integrity, the culture media was collected, and fluorescence intensity was measured using a plate reader. The presence of FITC signal in the media was interpreted as evidence of barrier leakiness.

To optimize needle quality, microinjection needles were prepared from 1-mm filament capillaries (World Precision Instruments) using a P-2000 laser-based micropipette puller (Sutter Instrument). A fine tip was pulled, and a 90° bend was introduced approximately 1.5 cm from the tip to facilitate precise injection.

Flow cytometry

Cryopreserved PBMCs and colon derived immune cells were thawed, washed, and counted. 100,000 cells per sample were allotted into FACS tubes, along with 20,000 cells for each fluorescence minus one (FMO) control and compensation control tube. All cells were incubated with FcR blocking reagent (Miltenyi) at a concentration of 1:50 for 5 min at room temperature protected from light. Cells were surface stained at 4°C, protected from light, using optimized concentrations of fluorochrome-conjugated primary antibodies for 30 min as well as live/dead fixable blue stain (ThermoFisher Scientific) at a concentration of 1:20 using the following antibody panels. The following fluorescence-tagged antibodies were used for PBMCs (see Star Methods Table for additional details): CD3 PerCP-Cy5.5, CD8 V500, CD45 RO-APC and LIVE/DEAD Fixable Blue Stain. Colonic immune cells were stained with the fluorescence-tagged antibodies: CD3 PerCP-Cy5.5, CD4 BUV395, CD8 V500, CD103 PECy7, S1PR1 PE, CD45RO APC, CD69 FITC and LIVE/DEAD Fixable Blue Stain. Colon epithelial cells from biopsy pinches and organoid cultures were stained with EpCam BV421. Cells were then washed in PBS and fixed using 4% PFA for 30 min at 4°C. Flow cytometry was performed on a BD Symphony (BD Biosciences, San Jose, CA) or 4 Laser LSR II and rainbow tracking beads (8 peaks calibration beads, Fisher) were used to ensure consistent signals between flow cytometry batches. Compensation controls for each surface antibody were prepared using anti-mouse IgG compensation beads. Analysis of flow cytometry data was performed using FlowJo software (version 10). Fluorescence minus one controls were used to inform gating.

Intracellular staining

Immune cells were in complete RPMI media for 6 hours in the presence of anti-CD107a, 1 μM GolgiStopTM (BD Biosciences), brefeldin A (5 μg/mL, Sigma Aldrich). Cells were incubated for 10 min in PBS with 0.5 mM EDTA prior to staining for surface markers and viability (Blue Viability dye, Invitrogen) for 20 min at room temperature. Cells were fixed in 4% PFA and permeabilized using FACS Perm 2 (BD Biosciences) prior to intracellular staining for IFNγ PE CF594, TNF BV786, perforin BV711 and granzyme B PerCPCy5.5. Colon epithelial cells from biopsy pinches (isolated as described before) and colonoid cultures (single cell suspension of epithelial cells were obtained by mechanical dissociation by 1X commercial TrypLE) were stained with cleaved caspase 3 APC post fixing and permeabilization. After staining, cells were re-suspended in 1% PFA and stored at 4°C in the dark until analysis within 24h. Apoptotic cells were identified as cleaved caspase 3^+ within gated populations of interest.

Immunofluorescence staining of pinch biopsies

Biopsies were immediately preserved in formalin in the endoscopy suite. Pinches were transferred to 70% ethanol after 24 hours and embedded in paraffin blocks. 4μm sections were used for analysis. Sections were de-paraffinized using Histoclear (National Diagnostics) and graded alcohols. Heat-induced epitope retrieval was performed in a DIVA decloaker (Biocare Medical) at 125°C for 30 seconds. Sections were stained with the antibodies overnight at 4°C. The following antibodies were used in 1:100 dilutions: E-cadherin, Cleaved caspase 3, Olfm4, KI67, CD45, CD8 and PPARγ (see Star Methods Table for additional details). Slides were washed in Tris-buffered saline (TBS) with 0.1% Tween-20 (TBST) and then incubated with 1:300 AlexaFluor-conjugated secondary

antibodies (ThermoFisher Scientific) for 2 hours at room temperature. Slides were washed with TBST, stained with NucBlue Fixed Cell Reagent (ThermoFisher Scientific), and mounted with ProLong Gold Antifade (ThermoFisher Scientific).

Microscopy and quantitative image analysis

Tissue specimens were imaged using the TissueFAXS whole slide scanning platform (TissueGnostics). For quantitative analysis, complete tissue areas were captured as digital grayscale images across five channels with filters for FITC, Cy3, Cy5, AF75, and DAPI. Cell phenotypes were identified and quantified using TissueQuest software (TissueGnostics), with thresholds established based on positive controls.

StrataQuest software (TissueGnostics) was utilized to measure cell-to-cell contact. The contact analysis application uses DAPI-stained nuclei to define the cytoplasm's inner boundary and extends outward to the plasma membrane. A three-pixel overlap between two cells within this defined region is required to meet the ''contact'' criterion. Reconstruction of images from 3D organoids and colonoid-T cell live imaging was done using Imaris software (Bitplane). For the reconstruction of images and 3D organoid quantification, Imaris software was utilized to process and analyze confocal and multiphoton microscopy images. Colonoids were imaged using a Zeiss LSM 900 confocal microscope, with z-stacks acquired at 1–2 μm optical sections to ensure high-resolution 3D reconstruction. Image files were imported into Imaris v9.5, where background subtraction and signal intensity normalization were performed. Surface rendering and volumetric measurements were conducted to quantify colonoid size, shape, and structural integrity. The "Surface" and "Spot Detection" modules were employed to segment individual colonoids and identify distinct cellular compartments based on fluorescent markers. Additionally, automated object tracking was applied to analyze dynamic changes in colonoid morphology over time. For statistical analysis, quantitative metrics such as volume, sphericity, and fluorescence intensity were extracted and compared between experimental conditions. Data were validated by independent blinded analyses to ensure reproducibility.

Distance measurement of T cells from epithelium

To quantify the spatial proximity of T cells relative to the epithelial layer, tissue sections were stained for epithelial markers (e.g., E-cadherin) and T cell markers (e.g., CD8). High-resolution fluorescence images were acquired using a confocal or widefield microscope. Image analysis was performed using ImageJ/Fiji software. A region of interest (ROI) was defined encompassing the epithelial boundary. The shortest linear distance from the centroid of each T cell to the nearest point on the epithelial surface was measured. StrataQuest was used for automated object segmentation and distance mapping to generate distribution plots and quantify mean or median distances across multiple fields.

Fatty acid oxidation assay

Flow cytometer sorted or magnetically enriched $CD8^+$ T cells from human colon were plated on a 24 well plate in 400 μL RPMI with 5mM glucose and allowed to incubate in a humidified 37°C incubator at 5% CO_2 overnight. 10% essentially fatty acid free BSA (Sigma Aldrich, A6003) in PBS was complexed at a volume ratio of 6.7:3 with palmitic acid-[9,10-^{3}H] (Pekin Elmer, NET043001MC) by vortexing for 60 s and was added at a 1:100 ratio to crypt media. This labelled medium was split into half and etomoxir (4 μM final) was added to inhibit FAO. 100 μl of the labelled FFA:PA:media mixture was added to the incubated cells, for a total volume of 500 μl, and were incubated for 1 hour, 37°C, 5% CO_2. Samples were removed from the wells and pelleted at 21K rcf. for 2.5 min. 400 μL of resulting supernatant was transferred to a filter column (Fisher Scientific) containing 3 mL of activated Dowex®1X8 resin (Sigma Aldrich). 2.5 mL of ddH_2O was added to elute ^{3}H-water from the column. 750 μL of eluent was added to 2.5 mL of EcoLume (MP Biomedicals). Beta-counts were measured on a scintillation counter (Beckman Coulter).

Bulk sequencing of human $CD8^+$ T cells

RNA isolation, library construction, sequencing, and alignment

$CD8^+$ T cells from PBMCs and colon ($CD103^+$ $CD69^+$ $CD8^+$) were FACS sorted directly into 50 μL of RLT Lysis Buffer (Qiagen) supplemented with 1% v/v 2-mercaptoethanol. Briefly, 50 μL of mixed lysate from each sample was transferred to a skirted 96 well plate. Genetic material was pulled down and purified by mixing the lysate in each well with 2.2x volumes of Agencourt RNAClean XP SPRI beads (Beckman Coulter) and washing 3x with 75 μL of 80% ethanol. After drying, the SPRI beads were re-suspended in 4 μL of pre-reverse transcription (RT) mix, incubated for 3 min at 72°C, and placed on ice. Next, Smart-Seq2 Whole Transcriptome Amplification (WTA) was performed: 7 μL of RT mix was added to each well and RT was carried out; then, 14 μL of PCR mix was added to each well and PCR was performed. Thereafter a cDNA cleanup was performed using 0.6x and 0.8x volumes of Agencourt AMPure XP SPRI beads (Beckman Coulter). cDNA was then quantified using a Qubit dsDNA HS Assay Kit (Life Technologies). Library size and quality were measured by Bioanalyzer using a High Sensitivity DNA Analysis Kit (Agilent Technologies). Sequencing libraries were prepared from WTA product using Nextera XT (Illumina). After library construction, a final AMPure XP SPRI clean-up (0.8 volumes) was conducted. Library concentration and size were measured with the KAPA Library Quantification kit (KAPA Biosystems) and a TapeStation (Agilent Technologies), respectively. Finally, samples were sequenced on a NextSeq500 (30 bp paired end reads) to an average depth of 5 million reads per library. Reads were aligned to hg38 (Gencode v21) using RSEM and TopHat and estimated counts and transcripts per million (TPM) matrices generated. Any samples with fewer than $5x10^5$ or more than $6x10^6$ aligned reads or fewer than 10,000 uniquely expressed genes were removed from subsequent analysis.

RNA-Seq Differential Expression Analysis

Differential expression analysis was performed using DESeq2 (v1.18.1). Expected counts from biological replicates for each cell type and participant were averaged prior to differential expression to prevent participant specific genes from generating false positives and reduce spurious heterogeneity from small (100-cell) populations. Small populations may show skewed expression based on the cell composition within; thus, this replicate averaging approach is particularly important given our limited access to tissue sources and low frequency of these immune populations in order to remove further bias from small population sorts.

Gene set analysis was performed using Ingenuity Pathway Analysis (IPA; winter 2019 Release, Qiagen Inc.) and Gene Set Enrichment Analysis (GSEA) using the piano package in R (1.18.1). For IPA, DEGs whose FDR corrected $q < 0.1$ were used in the "Core" analysis with the log2FC and q values included in the analysis. To implement GSEA on our DESeq2 results, we used the log2FC of all genes whose FDR corrected $q < 0.1$ as t-value input into the runGSA function with setting the argument geneSetStat = "gsea." We chose to use the KEGG and GO databases (downloaded from MSigDB v7.0) for GSEA analysis as these databases are well annotated for metabolic and cellular activation gene sets that are cell-type agnostic.

Seahorse mitochondrial metabolic analysis

Cell preparation and plating

The Agilent Seahorse XFp Cell Mito Stress Test was performed according to manufacturer's protocol using the seahorse XFp Analyzer. Peripheral and colon $CD8^+$ T cells were purified from PBMCs and colon immune cells, respectively, by positive magnetic cell separation. $CD8^+$ T cells were washed in XF medium, counted, and resuspended in XF medium at a concentration of $5x10^6$ cells/mL. $2x10^5$ cells/well were plated in a 96-well tissue culture plate, centrifuged at 1500 rpm for 5 min, and covered with 140 μL of XF medium. The plate was placed in a non-CO2 incubator overnight at 37°C.

Cartridge Preparation

200μL of calibrant was added to each well of the seahorse XF Cell Culture miniplate. The miniplate was coated with poly-D-lysine (Gibco) and incubated overnight at 37°C in non-CO2 conditions. Cells were transferred to the miniplate the following day.

Program Preparation

On day 2, the Mito Stress test was programmed in the seahorse console:

1. calibrate
2. equilibrate
3. Base line readings (3x loop)
4. Mix 1 → 3 min Wait → 2 min Measure → 3 min End
5. inject port B (3x loop)
6. Mix 2 → 3 min Wait → 2 min Measure → 3 min End
7. inject port C (3x loop)
8. Mix 3 → 3 min Wait → 2 min Measure → 3 min End
9. end

Reagents were prepared at the following concentrations: 1μM oligomycin, 1.5 μM FCCP, 100nM rotenone, and 1μM antimycin A. Drugs were then loaded into the delivery ports of the sensor cartridge with a multichannel pipette:

port B: 20μL oligomycin
port C: 22μL FCCP
port D: 24μL rotenone + antimycin A

Liposomal nanoparticles

Liposomes composed of 1,2-dioleoyl-sn-glycero-3-phosphocholine (DOPC, Avanti #850375), cholesterol (Avanti #700100), and 1,2-dioleoyl-sn-glycero-3-phosphoethanolamine-N-(Cyanine 5) (18:1 Cy5 PE, Avanti #810335) in a 51.5:38.5:10 mole ratio were synthesized by lipid film rehydration in PBS. The liposomes underwent six freeze/thaw cycles using liquid nitrogen to ensure unilamellarity and were subsequently extruded through a 100 nm and 200nm nm membrane to ensure even size distribution, which was confirmed via dynamic light scattering.

Liposomal nanoparticles and T cell culture

To assess lipid scavenging by TRM $CD8^+$ T cells, we co-cultured them with Cy5-PE-labeled liposomal nanoparticles designed to mimic plasma membranes. $CD8^+$ T cells were incubated with the labeled liposomes for 2 min at 37°C and immediately followed for imaging. Lipid uptake was then evaluated by measuring Cy5 fluorescence in $CD8^+$ T cells using confocal microscopy, indicating direct acquisition of liposomal lipids.

QUANTIFICATION AND STATISTICAL ANALYSIS

Data points represent biological replicates for mouse samples and individual participants in case of human samples and are shown as the means +/- SD. Statistical significance was determined as indicated in the figure caption using two-tailed, unpaired or paired Student's t tests or one-or two-way analysis of variance (ANOVA) (for greater than two comparison groups). Statistical details of each experiment can be found in the figure captions. *P* values of <0.05 were considered significant and represented by asterisk as follows: **P* 0.05, ***P* 0.01, ****P* 0.001, *****P* < 0.0001. Analyses were performed using Prism 9.0 (Graph-Pad software).

CellPress
OPEN ACCESS

Supplemental figures

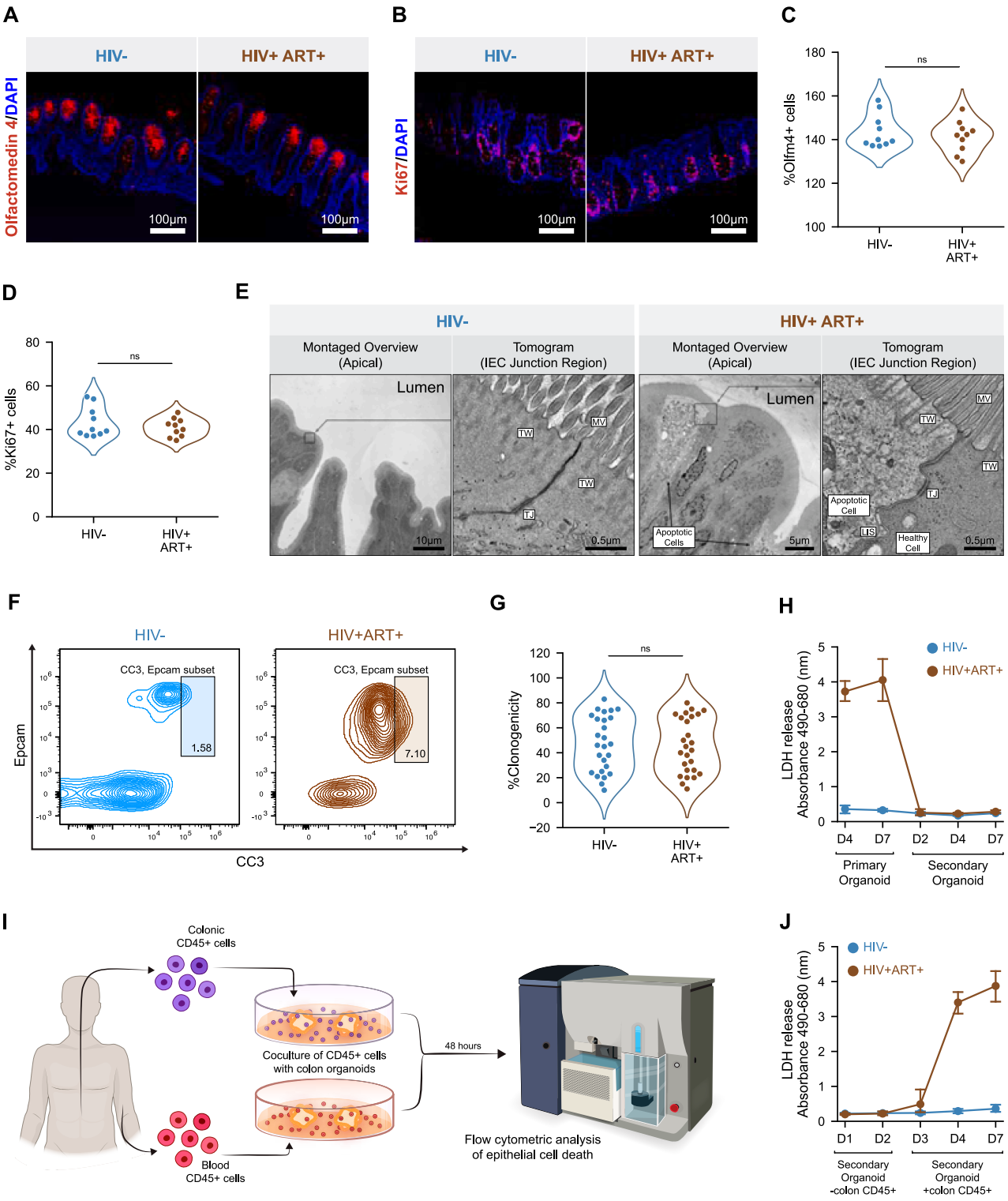

(legend on next page)

Figure S1. Increased epithelial cell death and impaired epithelial regeneration in the colonic mucosa of PWH on ART, related to Figure 1

(A) Confocal microscopy images showing epithelial progenitor cells (Olfactomedin4 in red) in colon biopsies from PWH on ART and HIV-uninfected individuals. Scale bars, 50 mm.

(B) Confocal microscopy images showing proliferative cells in the crypts (Ki67 in red) in colon biopsies from PWH on ART and HIV-uninfected individuals. Scale bars, 50 mm.

(C) Quantification of confocal imaging for colonic epithelial progenitor cells ($Olfm4^+$) in colon biopsies from PWH on ART and HIV-uninfected individuals. $n = 10$ per group.

(D) Quantification of confocal imaging for colonic epithelial proliferative cells ($Ki67^+$) in colon biopsies from PWH on ART and HIV-uninfected individuals. $n = 10$ per group.

(E) Electron tomographic images showing intact tight junctions in apoptotic epithelium of PWH on ART compared with HIV-uninfected individuals.

(F) Quantification of clonogenic potential of colonic epithelial cells from primary colonoids from PWH on ART and HIV-uninfected individuals. $n = 26$ per group.

(G) Representative flow cytometry plots of cleaved caspase 3 expression in epithelial cells ($Epcam^+$) in colon biopsies from PWH on ART and HIV-uninfected individuals.

(H) Spontaneous LDH release of primary vs. secondary colonoids from PWH on ART and HIV-uninfected individuals. $n = 5$ per group.

(I) Schematic depicting the isolation of autologous blood and colon-derived immune cells from study participants, followed by co-culture with the autologous secondary colonoids.

(J) Spontaneous LDH release of secondary colonoids from PWH and HIV-uninfected individuals after co-culture with autologous blood and colon immune cells. $n = 5$ per group.

(C, D, F, H, J) Data shown as mean ± SEM. Each point is one individual. ns, $p > 0.05$; $^*p < 0.05$; $^{**}p < 0.01$; $^{****}p < 0.0001$. Analyzed via t test.

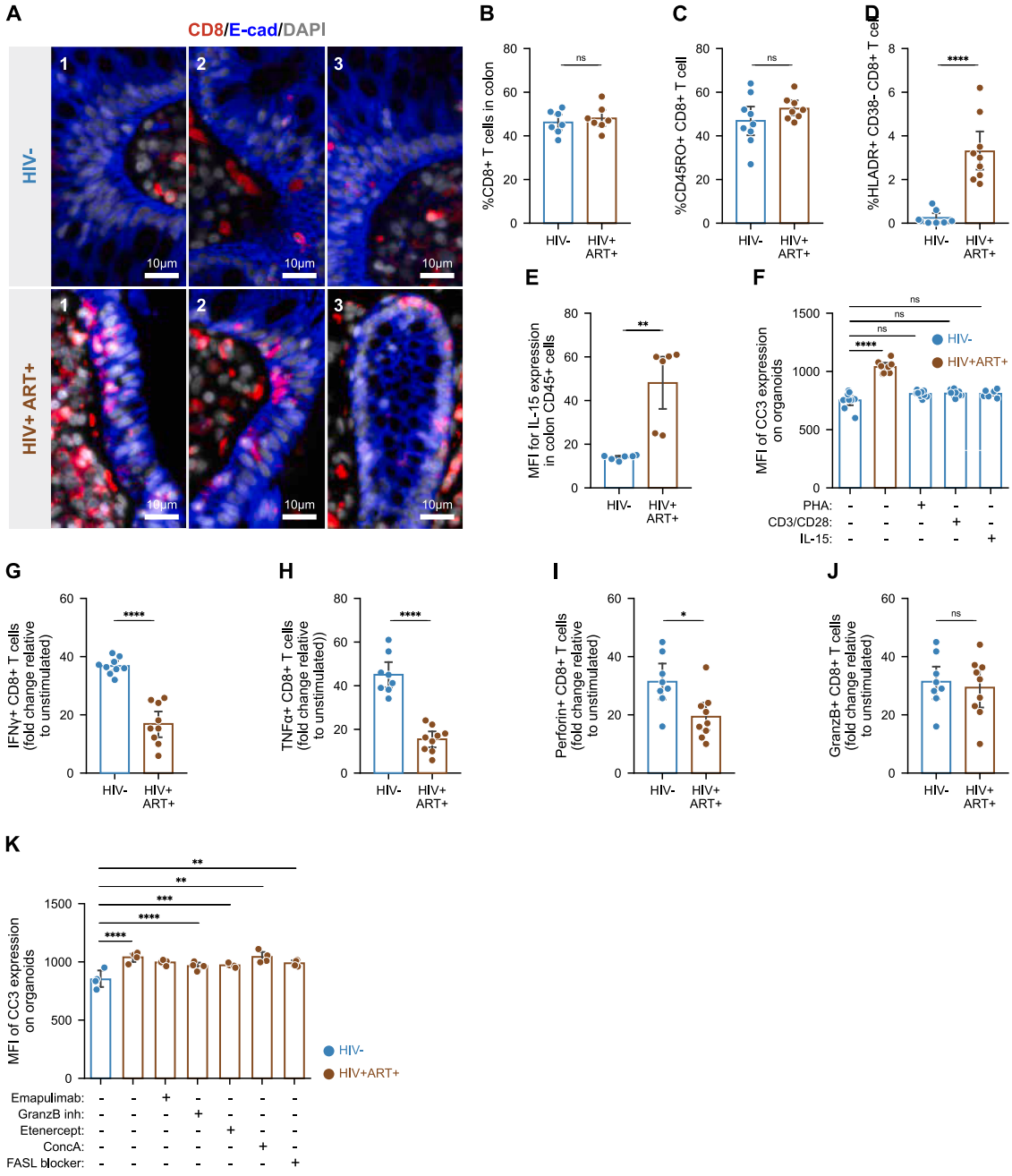

Figure S2. Cytotoxic and inflammatory reprogramming of colon TRM CD8$^+$ T cells in PWH on ART do not contribute to epithelial apoptosis, related to Figure 2

(A) Confocal microscopy images of colon biopsies showing the localization of CD8$^+$ T cells relative to the epithelial region; scale bar, 10 mm.

(B) Quantification of CD8$^+$ T cells (shows as percent of parent CD3$^+$ population) isolated from the colon of PWH on ART and HIV-uninfected individuals. *n* = 7 per group.

(C) Quantification of memory population of CD8$^+$ T cells (CD45RO$^+$ CD8$^+$) isolated from colon biopsies from PWH on ART and HIV-uninfected individuals. *n* = 9 (HIV$^-$), *n* = 8 (HIV$^+$ART$^+$).

(D) Quantification of frequency of late-activated colon TRM CD8$^+$ T cells (CD45RO$^+$ CD103$^+$ HLADR$^+$ CD38$^-$ CD8$^+$) from PWH on ART and HIV-uninfected individuals. *n* = 8 (HIV$^-$), *n* = 9 (HIV$^+$ART$^+$).

(E) Quantification of MFI of IL-15 expression between colon-derived total immune cells (CD45$^+$) from PWH on ART and HIV-uninfected individuals. *n* = 6 per group.

(F) Quantification of MFI (mean florescence intensity by confocal microscope) of cleaved caspase 3 expression in colonoids co-cultured with colon TRM CD8$^+$ T cells treated with PHA, CD3/CD28, and IL-15. *n* = 8 per group.

(G) Quantification of frequency of IFNg$^+$ colon TRM CD8$^+$ T cells in PWH on ART and HIV-uninfected individuals. *n* = 8 per group.

(legend continued on next page)

(H) Quantification of frequency of TNFa^{+} colon TRM CD8^{+} T cells in HIV-uninfected individuals and PWH on ART. n = 8 per group.
(I) Quantification of frequency of perforin^{+} colon TRM CD8^{+} T cells in HIV-uninfected individuals and PWH on ART. n = 8 per group.
(J) Quantification of frequency of granzymeB^{+} colon TRM CD8^{+} T cells in HIV-uninfected individuals and PWH on ART. n = 8 per group.
(K) Quantification of MFI (mean florescence intensity by confocal microscope) of CC3 expression in colonoids co-cultured with colon TRM CD8^{+} T cells treated with mAb for IFNg (Emapulimab), granzymeB inhibitor, TNF inhibitor (etanercept), perforin inhibitor (ConcanamycinA), or FASL blocker. n = 4 per group.
(B–K) Data shown as mean ± SEM. Each point is one individual. ns, $p > 0.05$; *$p < 0.05$; **$p < 0.01$; ****$p < 0.0001$. Analyzed via one-way ANOVA.

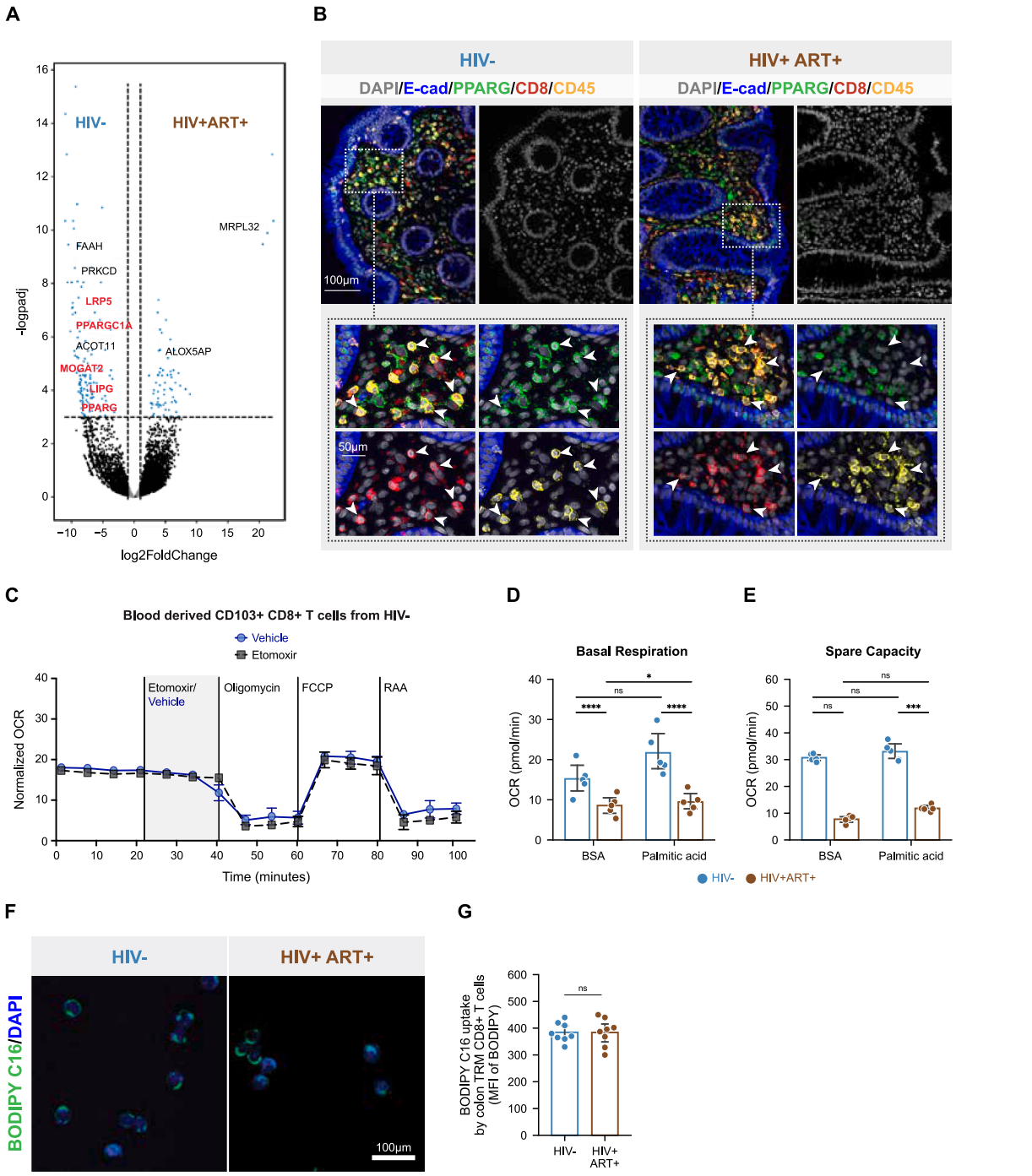

Figure S3. Metabolic impairment and reduced lipid uptake in colonic CD8⁺ T cells from PWH on ART, related to Figure 3

(A) Volcano plot showing downregulation of lipid-metabolism-associated genes in PWH on ART (n = 8) compared with HIV-uninfected individuals (n = 4) from individuals in Durban, South Africa.

(B) Confocal images of colon biopsies from PWH on ART and HIV-uninfected individuals showing PPARγ expression in CD8⁺ T cells and epithelium. Top: 100 mm scale; insets, bottom: 50 mm scale.

(C) Oxygen consumption rate (OCR, pmol/min/cells) of sorted, blood-derived CD103⁺ CD8⁺ T cells from HIV-uninfected individuals was measured using the Seahorse assay. The OCR was measured during the mitochondrial stress test with the addition of oligomycin, carbonyl cyanide p-trifluoromethoxy phenylhydrazone (FCCP), or rotenone and antimycin A (RAA). Results were normalized by the cell count. n = 5 per group.

(D) Basal OCR was calculated. n = 5 per group.

(legend continued on next page)

(E) Spare capacity was calculated. $n = 5$ per group.
(F) Confocal images of colon TRM CD8$^+$ T cells demonstrating fatty acid uptake capacity by internalizing BODIPY C16. Scale bar is 100 mm.
(G) Quantification of MFI of BODIPY C16 uptake by colon TRM CD8$^+$ T cells. $n = 8$ per group.
(C–E, G) Data shown as mean ± SEM. Each point is one individual. ns, $p > 0.05$; *$p < 0.05$; **$p < 0.01$; ****$p < 0.0001$. Analyzed via one-way ANOVA.

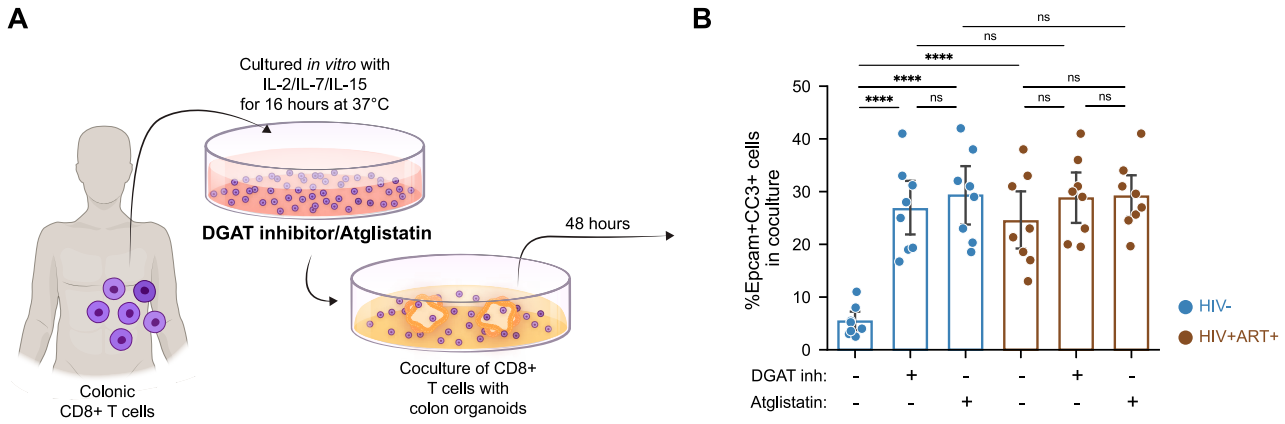

Figure S4. Modulation of lipid metabolism induces colon TRM CD8$^+$ T cells to mediate epithelial apoptosis, related to Figure 4

(A) Schematic showing colon TRM CD8$^+$ T cell treated with DGAT or ATGL (Atglistatin) inhibitors and then co-cultured with autologous patient-derived secondary colonoids.

(B) Flow cytometric quantification of epithelial apoptosis (Epcam$^+$ CC3$^+$) in co-culture, when colon TRM CD8$^+$ T cells from PWH on ART and HIV-uninfected individuals were treated with DGAT inhibitor or ATGL inhibitor (Atglistatin). $n = 8$ per group; data shown as mean ± SEM. Each point is one individual. ns, $p > 0.05$; *$p < 0.05$; **$p < 0.01$; ****$p < 0.0001$. Analyzed via one-way ANOVA.

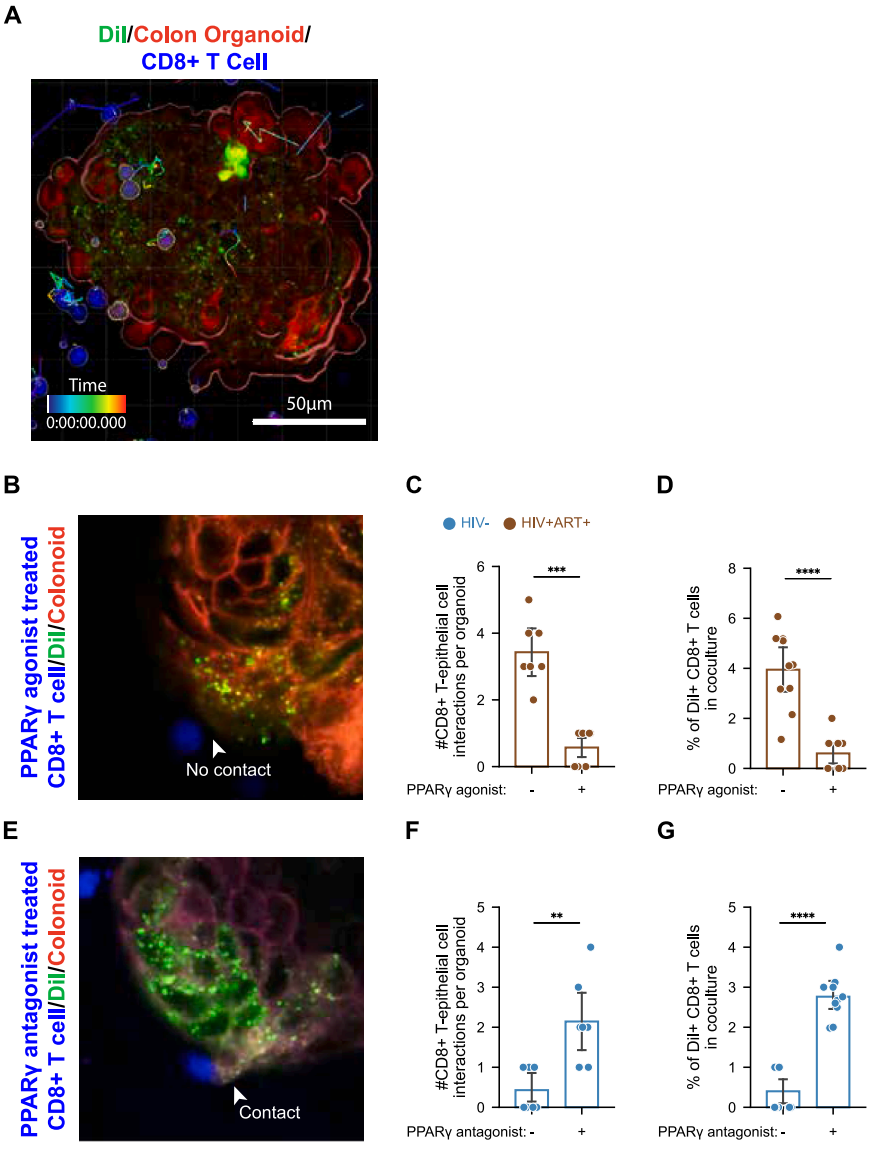

Figure S5. PPARγ modulation in colon TRM CD8⁺ T cells alters epithelial-CD8⁺ T cell interactions and lipid scavenging by colon TRM CD8⁺ T cells, related to Figure 5

(A) Live fluorescence confocal microscopy image showing epithelial cells stained with CellMask (red) and their lipids stained with DiI (green), co-cultured with colon TRM CD8⁺ T cells stained with CellTrace Violet (blue).

(B) Live fluorescence confocal microscopy image showing colon TRM CD8⁺ T cells co-cultured with colonoids with TRM CD8⁺ T cells (blue) derived from PWH on ART treated with PPARγ agonist.

(C) Quantification of the frequency of colon TRM CD8⁺ T cells interacting with epithelial cells in the co-cultures of PPARγ-agonist-treated colon TRM CD8⁺ T cells and autologous secondary colonoids derived from PWH on ART. $n = 7$ per group.

(D) Quantification of the frequency of DiI⁺ colon TRM CD8⁺ T cell in the co-culture of PPARγ-treated colon TRM CD8⁺ T cells and autologous secondary colonoids derived from PWH on ART. $n = 7$ per group.

(E) Live fluorescence confocal microscopy image showing colon TRM CD8⁺ T cells co-cultured with colonoids and TRM CD8⁺ T cells (blue) derived from HIV-uninfected individuals treated with PPARγ antagonist.

(F) Quantification of the frequency of colon TRM CD8⁺ T cells interacting with epithelial cells in the co-culture of PPARγ-antagonist-treated colon TRM CD8⁺ T cells and autologous secondary colonoids derived from HIV-uninfected individuals. $n = 7$ per group.

(G) Quantification of the frequency of DiI⁺ colon TRM CD8⁺ T cells in co-culture of PPARγ⁻antagonist-treated colon TRM CD8⁺ T cells and autologous secondary colonoids derived from HIV-uninfected individuals. $n = 7$ per group.

(C, D, F, G) Data shown as mean ± SEM. Each point is one individual. ns, $p > 0.05$; *$p < 0.05$; **$p < 0.01$; ****$p < 0.0001$. Analyzed via one-way ANOVA.

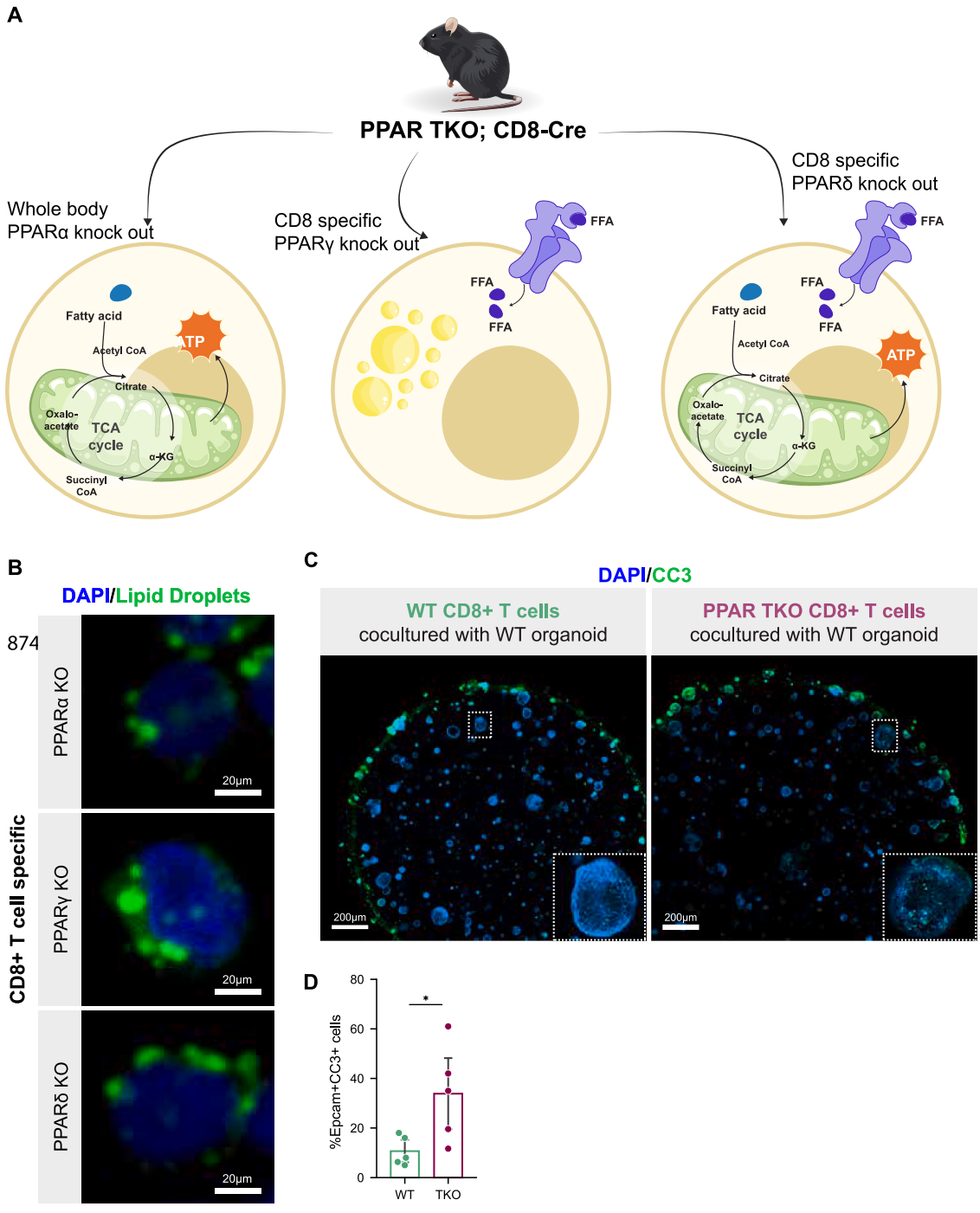

Figure S6. CD8⁺ T cell-specific deletion of PPAR disrupts lipid storage and enhances CD8⁺ T cell-mediated epithelial apoptosis, related to Figure 6

(A) Schematic showing the CD8⁺ T cell-specific knockout (KO) for PPARα, δ, and γ and α/δ/γ total KO (TKO).

(B) Confocal imaging of lipid droplets (green) in colonic CD8⁺ T cells from WT and CD8⁺ T cell-specific PPARα, δ, and γ KO mice. Scale bar, 20 mm.

(C) Confocal images of WT mouse colonoids co-cultured with colonic CD8⁺ T cells from WT and PPAR TKO CD8⁺ T mice. The cell death in the organoids is visualized by CC3 (green) and DAPI (blue). Scale bar, 200 mm.

(D) Quantification of flow cytometric analysis of colonic epithelial apoptosis (Epcam⁺ CC3⁺) from the colonoid cultures. $n = 5$ per group; Data shown as mean ± SEM. Each point is one mouse. ns, $p > 0.05$; *$p < 0.05$; **$p < 0.01$; ****$p < 0.0001$. Analyzed via t test.